M3LW-25OR0403033
Revision 0

Light Water Reactor Sustainability Program

Literature Review on Neutron Flux Effects on Aggregates and Minerals and Preliminary Use of Ion Irradiation to Investigate Flux Effects

Mohammed Alnaggar
Yann Le Pape
Yan-Ru Lin
Iyad Al-Qasir

September 2025

U.S. Department of Energy
Office of Nuclear Energy

ORNL/SPR-2025/4113
M3LW-25OR0403033

Literature Review on Neutron Flux Effects on Aggregates and Minerals and Preliminary Use of Ion Irradiation to Investigate Flux Effects

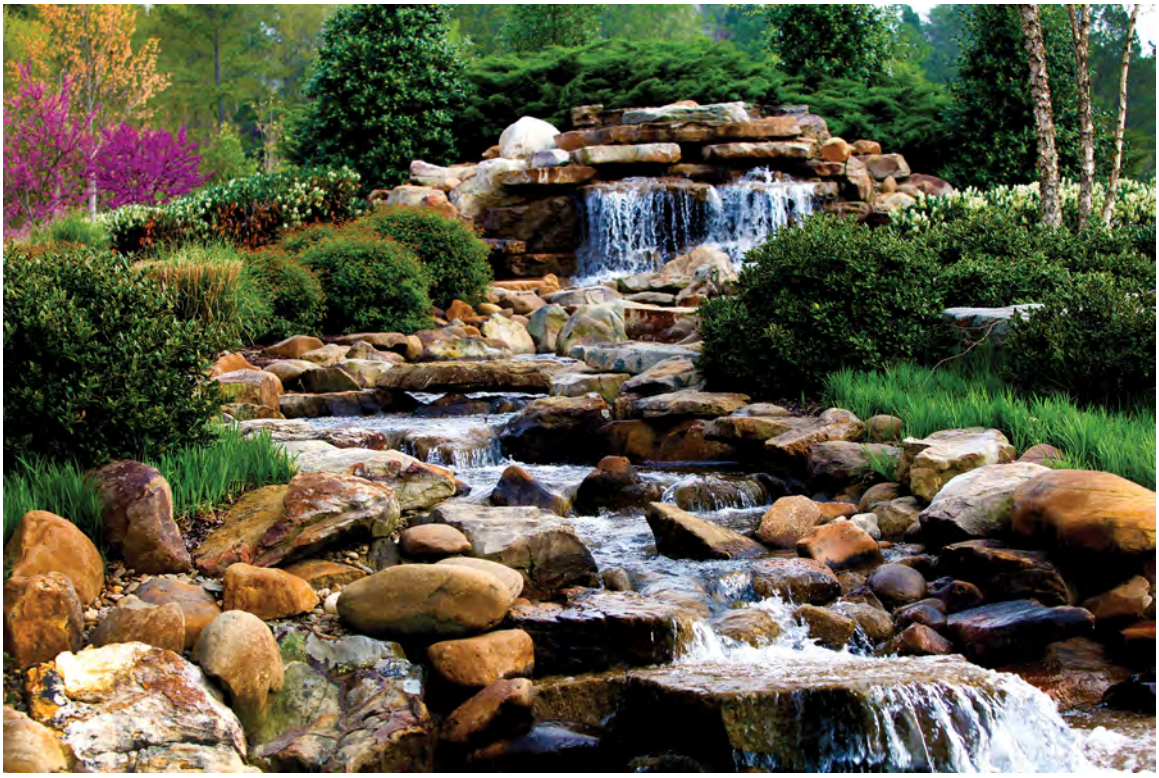

Mohammed Alnaggar
Yann Le Pape
Yan-Ru Lin
Iyad Al-Qasir

September 2025

ORNL IS MANAGED BY UT-BATTELLE LLC FOR THE US DEPARTMENT OF ENERGY

ORNL/SPR-2025/4113

Light Water Reactor Sustainability Program

M3LW-25OR0403033

Nuclear Energy and Fuel Cycle Division

LITERATURE REVIEW ON NEUTRON FLUX EFFECTS ON AGGREGATES AND MINERALS AND PRELIMINARY USE OF ION IRRADIATION TO INVESTIGATE FLUX EFFECTS

Mohammed Alnaggar
Yann Le Pape
Yan-Ru Lin
Iyad Al-Qasir

September 2025

Prepared by
OAK RIDGE NATIONAL LABORATORY
Oak Ridge, TN 37831
managed by
UT-Battelle LLC
for the
US DEPARTMENT OF ENERGY
under contract DE-AC05-00OR22725

CONTENTS

LIST OF FIGURES v
LIST OF TABLES vii
ABBREVIATIONS ix
EXECUTIVE SUMMARY 1
ACKNOWLEDGMENTS 3
1 INTRODUCTION 4
2 EVIDENCE OF FLUX RATE EFFECTS 5
3 POSSIBLE FLUX RATE EFFECTS ON COMMON CONCRETE AGGREGATE MINERALS . 7
3.1 Felsic Igneous Aggregates (Granite and Feldspar) 7
3.2 Mafic Igneous Aggregates (Basalt and Associated Minerals) 7
3.3 Metamorphic Minerals (Mica and Amphibole) 8
4 FURTHER INVESTIGATION OF RIVE IN QUARTZ 10
4.1 Defect Accumulation versus Self-Annealing Dynamics 10
4.2 Thermal Spike Behavior and Microstructure Development 12
4.3 Experimental Evidence at Low Temperatures 13
5 EFFECTS OF GAMMA IRRADIATION 14
5.1 Intrinsic Defects Induced by Gamma Irradiation in Silica 14
5.2 Extrinsic Defects and the Role of Impurities (H, OH, Cl, etc.) 15
5.3 Thermal Annealing of Gamma-Induced Defects in Silica 17
5.4 Dynamic Annealing under Simultaneous Irradiation and Heating 18
5.5 Summary of Gamma irradiation effects 18
6 IRRADIATION CREEP IN AMORPHOUS SILICA (a-SiO_2) 18
6.1 Experimental Observations at temperatures < 100 °C 20
6.2 Mechanisms of Radiation-Induced Creep in Silica 22
6.3 Comparison Across Irradiation Types 25
6.4 Quantitative Data and Threshold Conditions 27
6.5 Summary of Irradiation Creep observations 30
7 SUMMARY OF ORIGINS OF FLUX EFFECTS 31
8 ION IRRADIATION AS A MEANS TO INVESTIGATE THE INTERPLAY BETWEEN NEUTRON AND GAMMA RADIATION 33
8.1 Displacement Calculations 34
8.2 Electronic-to-Nuclear Stopping Power Analysis 35
8.3 Summary of insights from Ion irradiation and corresponding ENSP calculations 38
9 CONCLUSIONS AND PERSPECTIVES 38
10 RECOMMENDATIONS FOR FUTURE WORK 39

LIST OF FIGURES

Figure 1. Effect of neutron flux on irradiated aggregate expansion. 5
Figure 2. Schematic showing the hypothesized time-dependence effects on net observed damage. 6
Figure 3. Threshold displacement energy of silicon in quartz along various crystallographic directions, calculated using molecular dynamics simulations [43]. 33
Figure 4. Threshold displacement energy of oxygen in quartz along various crystallographic directions, calculated using molecular dynamics simulations [43]. 34
Figure 5. SRIM-calculated total ionization energy (electron stopping) versus depth for various ions implanted in quartz. 36
Figure 6. SRIM-calculated damage energy (nuclear stopping) versus depth for various ions implanted in quartz. 36
Figure 7. SRIM-calculated electronic-to-nuclear stopping power (ENSP) versus depth for various ions implanted in quartz. 37

LIST OF TABLES

Table 1. Irradiation Conditions in JEEP-II (Data from Tables 22–23 of Maruyama et al. [24]) and Experiment in LVR-15/XK1 from Le Pape et al. [20]. The multipliere in parenthes represent the relative ratio with respect to that of LVR-15/XK1 6

Table 2. Summary of defect types, annealing ranges, and mechanisms related to gamma irradiation 19

Table 3. Parameter settings for SRIM calculations of quartz (SiO_2) target 34

Table 4. Summary of ion irradiation conditions with a total fluence of 10^{21} m^{-2} 35

Table 5. Irradiation parameters from selected literature on quartz RIVE. 37

ABBREVIATIONS

a-SiO_2	amorphous silica
EPR	electron paramagnetic resonance
ESR	electron spin resonance
FFT	fast Fourier transform
IR	infrared
LWR	light-water reactor
MCNP	Monte Carlo N-Particles
NBOHC	non-bridging oxygen hole center
ODC	oxygen-deficient center
ORNL	Oak Ridge National Laboratory
OSL	optically stimulated luminescence
RIA	radiation-induced attenuation
RIVE	radiation-induced volumetric expansion
SEM	scanning electron microscopy
STE	self-trapped excitation
STH	self-trapped hole
TEM	transmission electron microscopy
TL	thermoluminescence
UTK	University of Tennessee, Knoxville
UV	ultraviolet

EXECUTIVE SUMMARY

Recent analysis of aggregate samples irradiated in high-flux reactors has shown evidence of flux effects. Aggregate from the same source that was irradiated at a medium flux showed less irradiation-induced volumetric expansion (RIVE) as compared to those irradiated in higher fluxes. Comparison of irradiation conditions of these reactors shows that temperatures are very similar—meaning that thermal effects cannot be responsible for the difference. However, not only were the neutron fluxes different; in some cases, gamma fluxes were also different and even opposite to the neutron fluxes. These complex irradiation conditions pose a challenge in understanding, and thus predicting, RIVE of aggregate and, by extension, concrete under operational conditions where neutron fluxes are much lower while gamma fluxes are not as low. Given that current estimates for concrete degradation due to irradiation are based on RIVE experimental data gathered from high neutron flux experiments, these estimates may be overly conservative. However, without a fundamental understanding of flux effects, such an assumption cannot be fully validated.

In general, RIVE is the macroscopic observation of density changes that result in a net reduction of aggregate minerals, aggregate, and concrete density under irradiation. However, this macroscopic expansion is a result of various lower-scale phenomena initiating at the molecular scale and propagating across scales. These phenomena are not always expansive. For example, self-healing of crystal defects can result in volume reductions. In addition, severe irradiation of already amorphous glasses can show volume reduction too. Other annealing processes can also result in volume reduction. Therefore, understanding the interplay of all of these phenomena from the molecular scale and up is key to developing a physics-based rather than phenomenological prediction of RIVE under various irradiation conditions.

This report details a comprehensive literature review of various athermal mechanisms that can correlate neutron and gamma irradiation as well as imposed stresses with damage and healing in aggregate minerals to best identify possible competing mechanisms that can explain the observed flux effects on RIVE. The report also presents the proposed use of ion irradiation as a qualitative surrogate method for evaluating the interplay between neutron and gamma effects. Here, it is assumed that the nuclear stoppage of ions corresponds to the neutron irradiation effects and the electronic stoppage of ions corresponds to gamma irradiation effects. A numerical study using the Stopping and Range of Ions in Matter (SRIM) software and a set of experimental evaluations are presented.

In summary, the findings in this report highlight the critical role of neutron flux, mineralogy, and associated recovery mechanisms in RIVE of concrete aggregate minerals. It was shown that higher neutron fluxes accumulate higher RIVE at fixed fluence levels, likely due to limited time for healing via pathways such as point-defect recombination, structural relaxation, and irradiation creep. Mineralogical variations were shown to dictate the degree of swelling, with quartz exhibiting the greatest flux sensitivity due to its amorphization behavior. Furthermore, gamma irradiation and stress-assisted mechanisms (irradiation creep) were shown to be possible contributors to flux-dependent recovery processes. A systematic simulation of ion-irradiation of quartz provided preliminary validation of RIVE dependence on the ratio between electronic and nuclear stopping power which serves as a qualitative surrogate for neutron and gamma irradiation effects.

Based on the observations and conclusions from the work documented in this report, the following activities are planned for FY 2026.

1. Develop analytical and/or computational predictive tools to quantify time-dependent defect

migration and healing in concrete aggregate minerals as functions of neutron radiation and gamma radiation using ion irradiation as surrogate experiments.

2. Perform ion irradiation experiments on Japan Concrete Aging Management Program aggregate with different ions and energies to represent similar neutron and gamma radiation effects.

ACKNOWLEDGMENTS

This research was sponsored by the US Department of Energy (DOE) Office of Nuclear Energy's Light Water Reactor Sustainability program Materials Research Pathway under contract DE-AC05-00OR22725 with UT Battelle, LLC / Oak Ridge National Laboratory (ORNL). The authors would like to acknowledge Professor Steven J. Zinkle, UTK-ORNL Governor's Chair Professor for Nuclear Materials, and Dr. Xiao-Ying Yu, Distinguished Scientist at ORNL, for their valuable discussions and insights.

1. INTRODUCTION

The concrete biological shield (CBS) provides radiological protection against reactor irradiation, including neutron and gamma radiation. Furthermore, different reactor designs depend on the CBS to provide support for the reactor pressure vessel (RPV) both during operational and accident conditions. Therefore, accurate understanding and prediction of the mechanisms that govern concrete degradation at extended operation are key in maintaining the safe and effective operation of current light-water reactors (LWRs) and for the possible recommissioning of previously decommissioned ones. Without such understanding, overly conservative levels of degradation that are based on accelerated irradiation conditions could limit future renewal of the current fleet of LWRs or present an economic barrier for restarting those that have been previously decommissioned.

To date, major accomplishments have been obtained by the Light Water Reactor Sustainability Program using test reactor data. To mitigate the conservatism resulting from accelerated irradiation conditions, it is critical to address time-dependent phenomena to complete enhanced integrity assessment of in-service irradiated concrete. Natural aggregate represents 60% to 70% of the concrete volume. Aggregate is a complex combination of various minerals formed under different conditions. Aggregate minerals' resistance against irradiation is characterized by the so-called *radiation-induced volumetric expansion* (RIVE). It was recently observed that this expansion is rate-dependent. Thus, the understanding and characterization of time-dependent phenomena such as flux and annealing effects on aggregate-forming minerals and irradiated cementitious material creep will provide stakeholders with insights into the mechanisms governing irradiation damage, as well as tools to assess potential concrete degradation at extended lifetimes.

In this report, evidence of flux effects will be presented, along with a detailed discussion of the literature regarding possible time-dependent mechanisms and hypotheses governing the observed RIVE dependence. In addition, this report presents a preliminary study that shows the possible use of ion irradiation as a surrogate to provide qualitative insights into such mechanisms.

2. EVIDENCE OF FLUX RATE EFFECTS

Neutron irradiation in nuclear environments displaces atoms in mineral lattices. These displacements are a result of neutrons colliding with the nuclei of the material's atoms; these collisions create cascade events. A typical measure of damage induced by neutron bombardment is the average number of displacements per atom (dpa); this can be estimated using methods like the Monte Carlo N-Particle Transport (MCNP) code, which uses statistical sampling to simulate the paths of particles as they interact with different materials.

These interactions represented by dpa produce point defects and eventually cause amorphization (metamictization) of crystalline aggregate minerals [21]. Under steady-state neutron flux at low temperatures (<100 °C), as encountered in LWR concrete, these defects accumulate with limited thermal annealing. The result is RIVE of aggregate minerals, which is often accompanied by microcracking and a loss of mechanical integrity [37].

Recent experimental data at test reactors show that at the same neutron fluence (i.e., dose) and irradiation temperature, the lower the flux (i.e., rate), the lower the damage (i.e., RIVE). This can be seen in Fig. 1 where the linear expansion due to irradiation of the same aggregate type at different reactor conditions is presented based on experiments from Maruyama et al. [24] and Le Pape et al. [20].

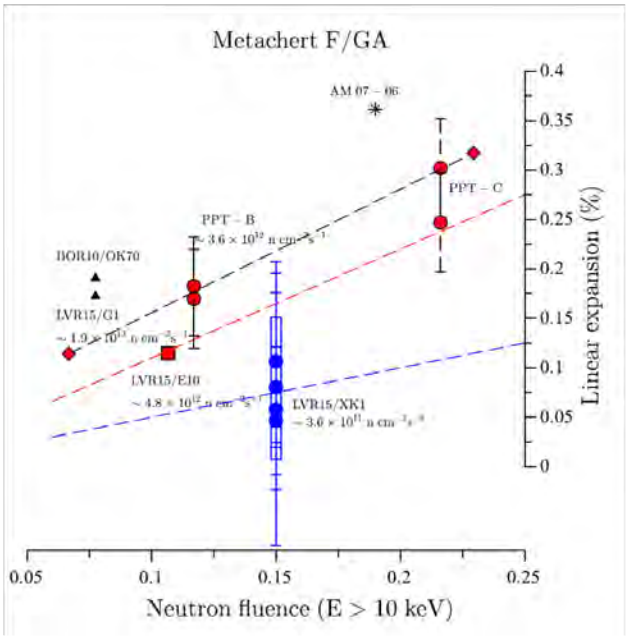

Figure 1. Effect of neutron flux on irradiated aggregate expansion.

The irradiation conditions for the presented aggregate expansion in Fig. 1 are listed in Table 1. A similar analysis was also presented in Maruyama et al. [25] that confirmed the presence of an obvious flux rate effect.

Because at the same fluence the dpa is expected to be identical, lower fluxes implicitly enable more healing. This conceptual hypothesis is illustrated schematically in Fig. 2. The major challenge is in identifying the different healing mechanisms and their possible dependence on the different conditions within these test reactors, including temperature, gamma doses, and stresses.

Table 1. Irradiation Conditions in JEEP-II (Data from Tables 22–23 of Maruyama et al. [24]) and Experiment in LVR-15/XK1 from Le Pape et al. [20]. The multipliere in parenthes represent the relative ratio with respect to that of LVR-15/XK1

	JEEP-II/PPT-B	**JEEP-II/PPT-C**	**LVR-15/XK1**
Fast-neutron flux (n·cm^{-2}·s^{-1}, E > 0.1 MeV)	~3.6 ×10^{12} (×10)	~3.6 ×10^{12} (×10)	~3.6 ×10^{11} (×1)
Fast neutron fluence (n·cm^{-2}, E > 0.1 MeV)	7.0 ×10^{18} (×0.57)	1.28 ×10^{19} (×1.05)	1.22 ×10^{19} (×1)
Gamma dose rate (kGy·h^{-1})	330 (×3.5–4.4)	290 (×3.2–3.9)	75.6–93.6 (×1)
Gamma dose (GGy)	0.2 (×0.15–0.22)	0.32 (×0.25–0.35)	0.9–1.3 (×1)
Irradiation temperature (°C)	53.3	53.3	~40–55
Duration, without outages (days)	~25 (×0.06)	~45 (×0.11)	~392 (×1)

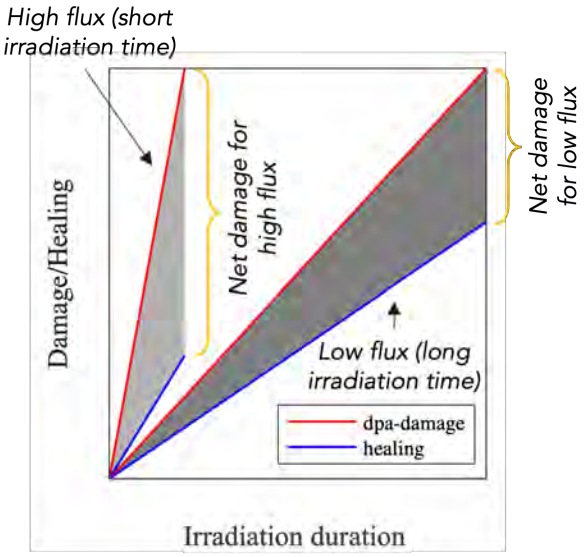

Figure 2. Schematic showing the hypothesized time-dependence effects on net observed damage.

3. POSSIBLE FLUX RATE EFFECTS ON COMMON CONCRETE AGGREGATE MINERALS

To understand the possible origins of flux rate effects, we begin by analyzing how different common concrete aggregates—feldspar, mica, amphibole, and rocks like granite and basalt—undergo RIVE. Different aggregates are categorized based on their geologic origins (felsic igneous, mafic igneous, metamorphic), and discussions of RIVE mechanisms and possible explanations of flux rate effects are presented.

3.1 FELSIC IGNEOUS AGGREGATES (GRANITE AND FELDSPAR)

Granite is a coarse-grained felsic igneous rock composed mainly of quartz and feldspars (e.g., orthoclase and plagioclase) with minor mica or amphibole. Its high-silica, fully polymerized silicate minerals make it particularly prone to radiation damage. Neutron irradiation breaks the strong covalent Si–O bonds in these tectosilicate frameworks, leading to significant volumetric swelling once the structure becomes amorphous [37].

For example, quartz (SiO_2) can undergo up to ~15–18% volume expansion when fully amorphized. Feldspars (aluminosilicate framework minerals common in granite) also swell appreciably (on the order of ~8% max RIVE) under high neutron fluence [37]. These large expansions stem from the rigid tectosilicate network: once displacement damage accumulates to a critical level, the crystal lattice collapses into a lower-density amorphous state.

The recent irradiation study on quartz in concrete aggregates by Maruyama et al. [25] demonstrated a pronounced dose-rate effect: for a given total neutron dose, a higher flux caused greater expansion, whereas a lower flux resulted in less swelling. The main observation at material crystal scale was that a fraction of the "distorted" crystal structure can recover, partially healing the damage and diminishing net expansion when the dose rate is low. The researchers postulated that the reason is that at lower flux, some irradiation-induced defects have time to recombine or anneal between collision events. By contrast, a high-flux bombardment overwhelms any defect recombination processes, driving the mineral into an amorphous, swollen state quickly. Feldspars are expected to exhibit a similar flux-dependent behavior: like quartz, they are framework silicates and will undergo amorphization-driven expansion. Within granite, differential swelling of its constituents (e.g., quartz expanding more than adjacent feldspar) leads to strain incompatibilities, often manifesting as microcracks at grain boundaries or through grains [37]. Overall, felsic igneous aggregates tend to have high RIVE but somewhat more homogeneous expansion behavior (dominated by quartz/feldspar) compared to multi-phase mafic rocks, as well as a marked flux rate sensitivity in their swelling due to the potential for defect healing at low dose rates.

3.2 MAFIC IGNEOUS AGGREGATES (BASALT AND ASSOCIATED MINERALS)

Basalt is a fine-grained mafic igneous rock, typically composed of lower-silica minerals such as plagioclase feldspar (calcium–sodium aluminosilicate), pyroxenes (single-chain silicates like augite), and sometimes olivine (isolated silica tetrahedra) or amphibole. Compared to felsic minerals, these mafic silicates have a greater proportion of ionic bonding and less polymerized structures, which influence their irradiation response. In general, highly ionic or less polymerized silicates exhibit lower volumetric swelling under neutron damage [37]. For instance, olivine and pyroxene, with more isolated or one-dimensional SiO_4 linkages, show much smaller RIVE (often only a few percent) at saturation, in contrast to the double-digit

expansion of quartz. Plagioclase feldspar in basalt is still a framework silicate and can undergo substantial amorphous swelling (comparable to other feldspars, up to several percent), but the absence of free silica (quartz) means basalt's overall expansion is moderated by its other components. Experimental data indicate that maximum RIVE decreases as the silicate structure becomes less cross-linked: swelling magnitudes follow the order quartz > feldspar > amphibole/pyroxene > olivine [37]. Thus, mafic aggregates like basalt tend to swell less in total than high-silica granite at an equivalent fluence.

However, the mineralogical heterogeneity of basalt plays a critical role in its degradation. Because basalt contains a mixture of phases with different radiation sensitivities (e.g., a feldspar grain may expand more than an adjacent pyroxene grain), neutron irradiation produces mismatch strains between phases. These internal stresses are often relieved by the formation of cracks along mineral interfaces or within grains [37]. As a result, basalt may suffer significant microcracking and mechanical property loss even if its net volumetric expansion is moderate. In fact, lower-silica (mafic) rocks can experience a sharp drop in elastic modulus for a given level of expansion because the uneven swelling induces further damage (voids, debonding) beyond the uniform lattice expansion [21].

The neutron flux effect is expected to influence basalt's behavior as well. At high flux (e.g., in accelerated irradiation tests), damage in the more susceptible basalt minerals (such as plagioclase) will accumulate quickly, potentially pushing those grains to amorphize and expand before adjacent less-sensitive grains have time to deform and thereby exacerbating stress concentrations. Under a lower flux (extended irradiation period), there is greater opportunity for defects in basalt's minerals to migrate to sinks (like grain boundaries) or for gradual strain accommodation, thereby reducing the net expansion and crack severity. Moreover, basalt's typically fine grain size (from rapid cooling) could aid defect annealing at low flux: grain boundaries in fine-grained mafic rock can act as sinks for point defects and thus improve radiation tolerance by recombination at interfaces [25]. It has been observed, for example, that larger crystal grains in aggregates exhibit less expansion than smaller ones under the same irradiation conditions, suggesting that microstructure size affects defect dynamics [25]. Overall, mafic igneous aggregates like basalt are somewhat less prone to extreme swelling but may be quite susceptible to flux-dependent cracking: a high flux can induce abrupt, uneven expansion and extensive microcracking, whereas a lower flux might allow more uniform, albeit still permanent, damage accumulation with fewer acute cracks.

3.3 METAMORPHIC MINERALS (MICA AND AMPHIBOLE)

Natural aggregates derived from metamorphic rocks often contain minerals such as mica and amphibole, which have distinct silicate structures and thus unique irradiation responses. Micas (e.g., biotite, muscovite) are sheet silicates (phyllosilicates) formed in metamorphic schists and gneisses (and also present as minor phases in some granites). Their structure consists of strongly bonded silicate layers separated by weaker van der Waals or ionic interlayer bonds (e.g., K^+ ions between sheets in muscovite). Under neutron irradiation, micas can undergo interlayer decohesion and amorphization of the sheets. The relatively weak bonds between layers make mica susceptible to delamination: radiation-induced defects and gas buildup can pry apart the layers, leading to an expansion perpendicular to the sheets and extensive microcracking along cleavage planes [38]. The in-plane silicate sheets, however, are covalently bonded and can also become amorphous with sufficient dose, which would increase volume within each layer. The net volumetric swelling of mica under high fluence can be significant, but it is likely anisotropic: larger in the c-axis direction, orthogonal to the sheets. Mechanical degradation in irradiated mica is characterized by embrittlement and loss of cohesion. Essentially, the crystal can split into a stack of damaged lamina. If mica-rich aggregates are present (e.g., mica schist pieces in concrete), neutron exposure can quickly reduce

their integrity. The influence of flux rate on mica's swelling may be substantial: at lower flux, there is more time for partial annealing of point defects within the sheets or for gradual stress relaxation via layer slip, potentially mitigating large sudden expansions. Conversely, a high flux could cause rapid amorphization of the sheet structure before any interlayer slip or defect recombination can occur, producing abrupt swelling and fragmenting of the mica. Although specific flux-dependent data on mica are scarce, the general principle (dose rate affecting defect accumulation vs. recovery) should apply: slower irradiation might allow the mica's layered structure to re-equilibrate to some extent between damage events, reducing macroscopic swelling. Nonetheless, even at low flux, eventually the mica will accumulate enough damage to amorphize; its capacity to "heal" is limited by the low temperature and the fact that broken interlayer bonds do not readily reform without thermal energy.

Amphiboles (a group of double-chain silicates, e.g., hornblende) are commonly found in metamorphic rocks like amphibolite and as minor constituents in igneous rocks. Their structure is intermediate: silicate tetrahedra form a double-chain backbone, with ionic bonds to various cations (Ca, Na, Mg, Fe, OH^- groups) between chains. Amphiboles thus have a mix of covalent and ionic bonding and a lower silica polymerization than feldspars but higher than pyroxenes. Under neutron irradiation, amphiboles can also become amorphous; their critical fluence for amorphization is on the order of 10^{19}–10^{20} n/cm^2 (fast neutrons) similar to other silicates [42]. The volumetric swelling upon full amorphization of amphibole is expected to be intermediate—likely a few percent to perhaps ~6–10%, extrapolating from its structural relatives (double-chain vs. single-chain silicates). Experimental observations on irradiated hornblende (a common amphibole) in aggregate form indicate it does expand, but it generally does so to a lesser extent than quartz/feldspar and more than purely ionic minerals. One key aspect is that amphiboles often contain hydroxyl (OH) groups in their structure; neutron and/or gamma irradiation can disrupt these as well, possibly contributing to defect mobility via radiolysis of OH or creating microvoids if water is released. The effect of flux on amphibole damage should qualitatively resemble that on other silicates: a high flux drives rapid defect accumulation and amorphization of the double chains, whereas a lower flux might allow some continuous recombination of Frenkel pairs or migration of defects along the chain structure. Amphiboles may have multiple crystallographic channels for defect movement (due to their double-chain tunnels), which could make them somewhat more radiation-tolerant at low dose rates than a fully rigid lattice. It is expected that metamorphic aggregates like amphibolite (which is composed of amphibole and plagioclase) would exhibit flux-dependent behavior combining both constituents; for instance, high flux could quickly amorphize plagioclase and amphibole, causing disparate swelling and cracking, whereas low flux might allow amphibole's defects to anneal enough to keep pace with plagioclase's slower expansion, yielding less cracking. Overall, the mineralogical and structural traits of metamorphic silicates (layered vs. chain structures) influence their susceptibility to radiation. Micas, with their planar weakness, may suffer early mechanical failure (delamination) even at moderate fluence, and amphiboles will swell and crack to an extent governed by their intermediate bonding character. Both types should see mitigated swelling at lower flux owing to some degree of defect recombination, though neither can escape eventual amorphization under prolonged neutron exposure.

4. FURTHER INVESTIGATION OF RIVE IN QUARTZ

Given the importance and large swelling of quartz, a more focused discussion of its RIVE mechanisms and the possible explanations of its observed RIVE dependence on flux rates are discussed here.

As previously mentioned, natural quartz (crystalline SiO_2) is known to swell under neutron irradiation due to radiation damage accumulating in its crystal lattice through collision cascades, gradually disordering the quartz structure as the dpa increases. Once damage surpasses a certain threshold, the crystalline quartz becomes partially or fully amorphous (metamict), leading to a density reduction of ~15% (from ~2.65 g/cm³ to ~2.2 g/cm^3)—equivalent to a volumetric expansion on the order of 15–18% [33].

Mechanistically, neutron impacts produce energetic primary knock-on atoms that generate displacement cascades in the quartz lattice [33]. Each cascade creates numerous point defects (Si or O vacancies and interstitials) and disrupted bonds. Some of these defects recombine immediately during the cascade's "thermal spike," but many survive, leading to cumulative damage. As irradiation continues, point defects can aggregate into defect clusters, voids, or dislocations, and the crystal's long-range order progressively degrades [33]. Ultimately, the quartz undergoes amorphization (loss of crystallinity) once the defect concentration is high enough, at which point large volumetric expansion is observed. This process is analogous to the metamictization of minerals: a crystalline quartz gradually becomes an aperiodic (amorphous) solid under intense neutron bombardment [33]. Microstructurally, irradiated quartz grains often exhibit internal microcracking once expansion strains build up. For example, scanning electron microscopy of neutron-irradiated quartz aggregates reveals extensive cracking in the post-irradiation state [25]. These cracks, along with any irradiation-induced nanovoids in the amorphous network, further contribute to the macroscopic volume change.

Next, a deeper analysis of possible explaining mechanisms for quartz is provided.

4.1 DEFECT ACCUMULATION VERSUS SELF-ANNEALING DYNAMICS

Recent studies have confirmed that high flux irradiation causes more swelling in quartz than low flux irradiation at the same total fluence [25]. This flux dependence was initially surprising, since at the same total fluence, it was usually assumed that the expansion is the same since the dpa is essentially the same. However, the rate of defect creation versus the rate of defect annealing seems to play a crucial role as hypothesized in Fig. 2.

It is expected that a possible explanation for the flux effect lies in the kinetics of defect accumulation and recovery. Under neutron irradiation at sub-100°C temperatures, quartz has very limited thermal annealing (since the temperature is low). However, even at these low bulk temperatures, some form of dynamic annealing or defect recovery may occur during irradiation when the dose rate is low. Essentially, at a lower neutron flux, there is more time between displacement events for the crystal to recover partial order or for point defects to annihilate before the next cascade arrives, as postulated in [25]. This reduces the net accumulation of permanent damage. At higher flux, by contrast, radiation damage is produced so rapidly that defects accumulate faster than they can recover. Surviving point defects from one cascade are quickly joined by new defects from subsequent cascades. The crystal lattice is driven toward amorphization before any significant defect recombination can occur. The result is a higher retained defect density and more extensive amorphous regions at a given fluence—hence greater volumetric expansion. It is important to emphasize here that any overlapping is assumed in space or location but not in time. In other words, even at very high fluxes, the probability that two cascades overlap at the same time is so low as to be nearly

impossible. However, a cascade occurring in a location where a previous cascade occurred is probable with high doses (fluences). This poses a challenge in using this simple argument as the only source for explaining flux effects though the degree of spatial overlap of cascades over shorter times that prevents in-between healing processes to occur.

Nevertheless, in this debate, one could argue that the observed flux effects may be due to any or a combination of the following processes: (1) longer time to reach the same fluence that allows more healing regardless of cascade overlaps; (2) inability to heal due to cascades overlapping (total dose dependent); or (3) self-healing processes dependence on irradiation.

If one focuses more on self-healing processes, it is interesting to find that specifically for quartz (and maybe for other aggregate minerals), several physical processes may contribute to this self-healing especially at lower flux:

- Point defect recombination and migration: Some fraction of the interstitial-vacancy pairs created in quartz can recombine if given time. Even at < 100 °C, certain point defects have enough mobility (or employ quantum tunneling or assistance from lattice strain) to migrate short distances. For instance, experiments have shown that radiation-induced paramagnetic defects in quartz (like unpaired electron centers) diminish upon room-temperature storage or low-temperature annealing, indicating gradual recombination or reconfiguration of defects [25]. A lower dose rate affords more time for a vacancy to meet an interstitial or for a broken bond to be chemically healed (e.g., by OH/hydroxyl impurities in natural quartz) before being frozen into an amorphous configuration. In the high-flux case, the rapid successive collisions "lock in" the defects faster than they can recombine, leading to a higher steady-state defect population.
- Structural relaxation (network relaxation): When quartz does become partially amorphous, the amorphous silica network can undergo slow relaxation or viscous flow given sufficient time. Recent ion-irradiation studies on quartz have identified a low activation energy process (~0.13 eV) associated with viscous flow or rearrangement in the amorphized SiO_2 network [29]. This means that even at modest temperatures (room temperature to 60–90 °C), the disordered regions can very slowly compact or reorganize if not continuously bombarded. Such relaxation can reduce internal stresses or densify the amorphous regions slightly, counteracting some swelling. Under a high flux, however, the continuous bombardment disrupts any nascent relaxation; in fact, it may drive further dilation (as new damage creates additional free volume faster than the network can relax). The net effect is that slow irradiation allows the amorphous structure to settle into a lower-volume configuration than fast irradiation does [29].
- Cascade-induced annealing: Paradoxically, the radiation itself can aid defect healing under certain conditions. Each fast neutron impact generates a thermal spike: a tiny, transient hot region along the cascade (10^4–10^5 K for a few picoseconds in a nanometer-sized volume). In quartz, these thermal spikes tend to cause localized melting and immediate quenching. Primak (1958) noted that thermal spikes allow displaced atoms to be accommodated by local structural deformation rather than creating permanent voids [34]. Specifically, the intense local heat can momentarily drive the quartz structure into a high-temperature polymorph or disordered state (analogous to the β-quartz phase or a molten state) and then quench it. This process can produce a "minor reorientation of the Si–O tetrahedra without extensive disruption of the structure," effectively a form of instantaneous self-annealing within the cascade [34]. The damage thus accumulates gradually as many such partial disordering events build up. At lower flux (longer intervals between cascades), each cascade's

thermal spike affects a relatively pristine or partly healed region, and the material might take longer (more total fluence) to reach the critical level of disorder. At higher flux, cascades occur in regions that may still be in a metastable disordered state from previous hits, so the damage can accumulate more efficiently (cascades "piggyback" on each other's remaining disorder). In essence, cascade overlap in space at high flux would happen over short time intervals, leading to accelerated amorphization. Meanwhile, at low flux the quartz lattice between events can slightly re-order (within the constraints of low temperature), delaying the amorphous transition.

- Delayed amorphization threshold: Because of the above factors, the critical dose (fluence) required to amorphize quartz is higher at lower flux. This is similar to the effect of raising irradiation temperature. Indeed, raising the irradiation temperature has long been known to delay quartz amorphization by allowing defect annealing; for example, data compiled by Bykov et al. [4] show that increasing irradiation temperature from 25 °C up to ~200 °C shifts the onset of quartz expansion to higher neutron doses due to annealing of point defects [33]. (Above ~200 °C, substantial in situ annealing can occur, greatly reducing damage accumulation [33].) While temperatures below 100 °C were historically thought to be too low for significant annealing [33], the flux effect demonstrates that time can substitute for temperature to some extent. A low flux at 60 °C can mimic the effect of a somewhat higher temperature irradiation by giving defects a chance to recombine. In summary, under steady-state irradiation at <100 °C, a slower damage rate leads to a lower equilibrium defect density: the material spends more time in partial recovery modes between damage events, resulting in less final expansion for the same total fluence [25].

4.2 THERMAL SPIKE BEHAVIOR AND MICROSTRUCTURE DEVELOPMENT

Beyond point-defect kinetics, neutron flux can influence how the microstructure evolves via cascade events. Each displacement cascade (a series of atomic collisions) deposits energy in a small region, causing thermal spikes and intense local excitation. In quartz, as noted, thermal spikes tend to cause local, rapid restructuring rather than immediate, gross void formation [34]. The damaged zone typically solidifies into an amorphous pocket or a highly strained configuration of SiO_2. If the irradiation flux is high, new cascades may hit these partially disordered pockets before they can relax or before surrounding crystalline regions can heal them. These overlapping cascades can drive the region to a fully amorphous state more quickly. They might also induce secondary effects like linking of damaged zones or growth of defect clusters. For instance, overlapping damage can lead to the formation of nanometer-scale voids or bubbles in quartz: oxygen atoms knocked out of the lattice might pair up into O_2 molecules and get trapped, creating tiny voids, while silicon interstitials aggregate elsewhere [33]. High flux accelerates such clustering because it maintains a high concentration of mobile defect species in a local area at one time. At lower flux, the chances of one cascade directly overlapping the exact site of a recent, previous cascade are much lower (since the time between events is larger relative to the cooling and relaxation time of a cascade region). Thus, the damage tends to be more homogeneously distributed and in smaller pockets. This can affect volumetric expansion: a highly overlapped, amorphous region might swell slightly more (due to extra free volume or nanovoids) than many isolated amorphous pockets that remain surrounded by crystalline constraints. In addition, a slower irradiation allows strain redistribution; the crystal may undergo gradual internal strain accommodation instead of forming as many microcracks. In a high-flux scenario, the quartz crystal experiences a rapid buildup of lattice strain as it amorphizes, often leading to brittle fracture of the crystal lattice in the form of microcracks to relieve stress. Those cracks contribute to expansion (since the crystal "opens up"), but they also can absorb some strain energy. In a low-flux

scenario, microcracking may be less pronounced or occur later because the expansion happens more gradually, sometimes allowing the lattice to elastically accommodate more strain before cracking. To summarize the microstructural perspective: high neutron flux drives quartz more quickly toward a heavily damaged, amorphous state with associated voids and microcracks, whereas lower flux leads to a more moderate damage state where some crystalline order remains longer, and defect-induced expansion is partially mitigated by ongoing recovery processes. Consequently, the steady-state swelling (volume change at a given fluence) is higher in the high-flux case.

4.3 EXPERIMENTAL EVIDENCE AT LOW TEMPERATURES

Experiments confirm these mechanisms in natural quartz and similar silicates under low-temperature irradiation. In quartz irradiated below 100°C, flux-dependent swelling has been directly measured: for example, quartz samples irradiated in a test reactor at $\sim 10^{12}$ n/cm^2·s versus $\sim 10^{13}$ n/cm^2·s (one order difference) showed significantly different volume expansions for the same total neutron fluence [25] (See Fig. 1). The higher-flux condition produced a larger expansion, consistent with less defect annealing time. In situ monitoring and post-irradiation analyses (X-ray diffraction, dilation measurements) revealed that low-flux irradiated quartz retained more crystallinity (lower amorphous fraction) than a high-flux counterpart at the same fluence, correlating with the smaller strain.

Furthermore, ion irradiation studies support the idea of defect relaxation at low rates given that results show continued viscous flow, even at low temperatures, can recover part of the damage [29]. This aligns with neutron observations: under a slow, steady irradiation at low temperature, the amorphous regions in quartz may undergo some compaction (viscous flow or other athermal relaxation), whereas a fast, intense irradiation drives continuous expansion without giving the structure time to adjust.

5. EFFECTS OF GAMMA IRRADIATION

Gamma radiation can introduce a variety of point defects in amorphous silica, including silica found in natural geologic materials and aggregates. These high-energy photons primarily cause ionization and excitations in SiO_2, breaking Si–O bonds and producing complementary defect pairs. The two principal intrinsic defects are silicon dangling bonds (known as E′ centers) and non-bridging oxygen hole centers, NBOHCs (≡Si–O•) [8]. In natural silica (e.g., volcanic glass, opaline silica, or siliceous aggregates), these defects form similarly to those in synthetic vitreous silica, though impurity content (e.g., H_2O/OH vs. Cl) can modulate their creation and annealing.

5.1 INTRINSIC DEFECTS INDUCED BY GAMMA IRRADIATION IN SILICA

E′ Centers (Silicon Dangling Bonds).

The E′ center is a paramagnetic defect consisting of a three-coordinated silicon with an unpaired electron (≡Si•). Gamma irradiation in amorphous SiO_2 creates E′ centers by cleaving Si–O bonds, typically via radiolytic generation of electron–hole pairs (excitons) that localize on a Si–O–Si linkage and cause it to break [22]. The result is a Frenkel-type pair: a silicon dangling bond (E′) and a complementary oxygen dangling bond (hole center). These defect pairs often originate from pre-existing strained bonds in small ring structures of the silica network [8]. Experimental and simulation studies show that gamma irradiation tends to convert larger rings (6–7 membered) into 3- or 4-membered rings, which are highly strained; breaking such a ring produces an E′–NBOHC pair [8]. The E′ center is identified by a characteristic electron paramagnetic resonance (EPR) signal ($g \approx 2.001$) [2]. In natural or pure silica glass with low impurity content, E′ centers can reach densities detectable by EPR and cause significant UV transparency loss under high gamma dose [8]. Importantly, E′ defects in silica are intrinsic to the SiO_2 network (an "oxygen-vacancy" type defect) and serve as electron traps.

Non-Bridging Oxygen Hole Centers (NBOHCs)

The NBOHC is the complementary intrinsic defect to the E′ center. It is essentially a three-coordinated oxygen with a dangling bond (≡Si–O•), carrying a hole on the oxygen. NBOHCs form when a Si–O–Si bond is broken and one electron remains with the silicon (forming E′) while the oxygen is left with an unpaired hole. Like E′ centers, NBOHC formation is strongly linked to the presence of strained bonds and small rings in the glass structure [8]. NBOHCs are paramagnetic with a typical electron spin resonance (ESR) signal of $g \approx 2.008$ and are well-known for their optical luminescence: they emit a broad red photoluminescence band peaking around ~1.9 eV (~650 nm) [12]. In absorption spectra, NBOHCs contribute to bands in the blue/UV (e.g., a band near 4.8 eV has long been associated with oxygen hole centers) [10]. Together with E′ centers, NBOHCs are a fundamental cause of gamma-induced optical darkening in silica: as gamma dose increases, the synchronized growth of E′ and NBOHC defect populations leads to increased absorption from the UV into the visible [8]. This paired generation is so consistent that in pure silica the concentrations of E′ centers and NBOHCs track one another linearly with dose [22] (reflecting their origin as complementary halves of the same broken bonds).

Other Intrinsic Defects and Precursors

Amorphous silica can also host other radiation-related defects, though often in smaller concentrations. Oxygen-deficient centers (ODCs) are defects where an oxygen is missing from the network; they can be precursors to E′ centers. For example, a neutral oxygen vacancy (two Si atoms bonded to each other) is an ODC that is non-paramagnetic but can absorb UV light (one such ODC type gives the "D-band" around 5 eV) [22]. Gamma photons can ionize these ODC precursors, converting them to paramagnetic E′ centers (Si•) plus released electrons [22]. Another intrinsic species observed after high-dose irradiation is the peroxy radical (≡Si–O–O•, sometimes called POR), which occurs when an interstitial O_2 molecule attaches to a silicon dangling bond. This effectively converts an E′ center into a peroxy radical. Peroxy radicals have an ESR signature distinct from NBOHCs (typically $g \approx 2.011$) and are associated with an optical absorption band near 4.4–5.0 eV (often overlapping with other bands) [22]. They also exhibit luminescence (e.g., a blue-violet emission around 4.3 eV in some studies) [22]. Radiolytic O_2 needed for peroxy defects can be created in silica by gamma irradiation via Frenkel pair formation (an oxygen atom displaced into an interstitial void) [22, 32]. In fact, interstitial O_2 molecules are readily observed in irradiated amorphous SiO_2 by their distinctive infrared luminescence at 1272 nm (the $O_2(^1\Delta \rightarrow {}^3\Sigma)$ transition), and their presence depends on the available free volume in the glass [32]. Pristine silica glass (density ~2.20 g/cm^3) can accommodate radiolytic O_2 even at MGy-level doses, whereas crystalline quartz cannot [32]. Thus, amorphous silica can both produce and trap O_2 upon irradiation, enabling peroxy radical formation especially during annealing. Another transient intrinsic defect worth noting is the self-trapped hole (STH)—a hole localized on a bridging oxygen (≡Si–O–Si≡ with one O^-). STHs in bulk silica were identified via ESR at low temperatures [19]. They are thought to be immediate hole traps after gamma excitation, and while at room temperature many STHs further evolve (e.g., by breaking a bond to become stable NBOHCs [22]), some fraction may persist in low-temperature or high-dose conditions. Overall, E′ centers and NBOHCs are the dominant long-lived intrinsic defects in irradiated amorphous SiO_2, and their concentrations and interactions largely determine the material's radiation response.

5.2 EXTRINSIC DEFECTS AND THE ROLE OF IMPURITIES (H, OH, CL, ETC.)

Hydrogen / Hydroxyl Impurities

Many natural amorphous silicas (e.g., opal, volcanic glass, or silica in aggregates) contain substantial –OH groups (silanols) or molecular water in their structure. Under gamma irradiation, Si–OH bonds can be broken, yielding an NBOHC and a hydrogen atom [28]. For instance, one proposed mechanism is: Si–OH + $\gamma \rightarrow$ Si–O• (NBOHC) + H• [28]. The free H atoms produced by radiolysis tend to quickly pair up into H_2 molecules (especially in the interconnected free volume of amorphous silica) [28]. Concurrently, gamma rays can also break Si–H bonds (if present) in a hydrogen-impregnated silica, similarly releasing H• radicals and E′ centers [28]. Thus, wet silica tends to generate E′ centers accompanied by molecular hydrogen: experiments with UV or gamma irradiation show that in "wet" fused silica, E′ centers are generated together with H_2 in a 2:1 ratio (one H_2 per two E′, consistent with two Si–H or Si–OH precursors yielding one H_2) [28]. These radiolytic H_2 molecules are not benign bystanders—they actively participate in defect annealing (next section). In addition, hydrogen can form its own paramagnetic centers: the H(I) center is a defect where a hydrogen atom is bonded to a silicon (≡Si–H) with an unpaired electron on Si. This often results from an E′ center reacting with H_2 or H• (E′ + $H_2 \rightarrow$ Si–H (H(I)) + H•) [22]. H(I) centers have been detected by ESR, showing hyperfine interactions indicative of a proton bound to the silicon dangling bond [22]. Extrinsically, the presence of hydrogen generally tends to reduce the net

concentration of E′ and NBOHC defects under irradiation because many of the broken bonds quickly get terminated by H atoms. Comparative studies of "wet" vs "dry" silica show that silica with high OH content produces fewer unrelaxed E′ centers; instead, one observes growth of Si–OH groups after irradiation (via NBOHC + H → Si–OH) [27]. Infrared spectroscopy on gamma-irradiated natural silica indeed finds an increase in the Si–OH stretch absorption band, confirming that some non-bridging oxygen atoms convert to silanols during or after irradiation [27]. In summary, hydrogen impurities introduce alternate defect pathways: rather than leaving behind only dangling bonds, gamma irradiation in H-rich silica tends to create silanol groups and H-related centers. These extrinsic processes play a crucial role in annealing (often healing defects even at ambient temperature).

Chlorine Impurities

Chlorine is commonly present in synthetic silica (from $SiCl_4$ precursors), but natural silica typically has much lower Cl content. When present, chlorine gives rise to its own radiation-induced defects. In chlorine-doped silica glass, gamma rays can cause Si–Cl bond cleavage, releasing a chlorine atom ($Cl^{\cdot}$) and creating a silicon dangling bond (E′) [22]. The atomic chlorine defect (Cl^0) is paramagnetic and has been observed by optical and ESR techniques. Radiation-induced Cl^0 centers manifest optical absorption bands in the near-UV; e.g., new absorption around ~3.3–3.8 eV (330–380 nm) appears in irradiated Cl-containing silica [22]. These bands have been attributed to chlorine-related species (such as Cl^0 or Cl_2^-) created by the detachment of Cl from the silica matrix [22]. A specific example is the formation of dichlorine molecules (Cl_2) in the glass: two Cl radicals can pair up to form Cl_2, which can be trapped in microscopic voids. Cl_2 is not paramagnetic but does absorb in the UV (around 3.8 eV). Another known extrinsic center is the E'_δ center, a variant of the E′ center associated with the presence of chlorine (and/or other network modifiers); Cl in the vicinity of a dangling bond can delocalize the unpaired electron (a "delocalized E′" center) [18]. Chlorine-related defects are important in optical fiber contexts because they contribute to radiation-induced attenuation in the UV–visible domain [22]. They do not naturally recombine as easily as hydrogen-related defects; instead, their annealing often requires high temperature (to mobilize Cl for recombination or out-diffusion). Natural silica aggregates usually have negligible chlorine compared to synthetic fiber–grade silica, so Cl extrinsic effects are more a point of comparison. Overall, chlorine impurities tend to introduce long-lived color centers under gamma irradiation, which need vigorous annealing to remove.

Metal and Other Impurities

Natural siliceous materials often contain trace amounts of aluminum, alkalis, or other cations. These impurities can trap radiation-induced charges and form extrinsic centers. In amorphous silica, Al impurities can capture holes or electrons; ESR studies have co-observed Al-related centers (e.g., Al^0, $[AlO_4/H]^0$) [18]. These have their own annealing behavior—e.g., an Al-hole center may be stabilized by Na^+ and only anneal when those charges migrate [18]. Such extrinsic traps can reduce the yield of intrinsic E′/NBOHC centers and create additional TL/OSL signals. Typically, these extrinsic centers have high thermal stability (often requiring hundreds of °C to anneal). Here we primarily emphasize H and Cl because they are directly involved in the annealing reactions of the main intrinsic defects.

5.3 THERMAL ANNEALING OF GAMMA-INDUCED DEFECTS IN SILICA

E′ Center Annealing

In dry, impurity-free silica, E′ centers are quite stable at room temperature. Significant thermal annealing typically begins at several hundred °C. Isochronal studies show E′-associated bands and ESR remain near initial levels up to ~150 °C, then diminish around 200–300 °C, with major loss by 400–500 °C [45]. By ~500–600 °C (tens of minutes), most E′ centers are gone (without continual radiation) [45]. This suggests an intrinsic activation energy on the order of 1.5–2 eV for direct recombination in dry silica [31]. However, if hydrogen or water is present, E′ centers anneal at much lower temperatures via chemical reaction. In an H_2O atmosphere, E′ centers predominantly anneal in the range 150–300 °C, with mean activation energy ≈ 1.23 eV for the E′+H_2O reaction (reaction-limited kinetics) [31]. In hydrated or "wet" silica, even at room temperature some E′ centers disappear over time via reaction with mobile H_2 produced by radiation [27]. Messina et al. observed that in gamma-irradiated silica (up to ~0.6 kGy), a significant fraction of E'_γ centers decayed spontaneously at room temperature once irradiation ceased; within an hour, UV transparency recovered, consistent with E′ + H_2 → Si–H [27]. At higher doses ($\gtrsim$ 10s kGy), room-temperature annealing becomes slower, and IR shows a concurrent increase in Si–OH, implicating water-related chemistry in the slow stage [27]. In summary, pure thermal annealing of E′ requires high T (~400°C+), but impurity-assisted annealing (H_2/H_2O) can eliminate E′ at much lower T or even ambient over time [27][31]. End states are restored Si–O–Si bonds (if recombining with NBOHC) or terminated bonds like Si–OH / Si–H (if reacting with H species) [22].

NBOHC Annealing

NBOHCs tend to be less stable than E′ upon heating. Even in dry silica, NBOHCs begin to anneal at somewhat lower temperatures. For instance, femtosecond-laser induced NBOHC defects disappeared after ~10 h at 300 °C, whereas E′ required ~600 °C for complete removal [45]. In many studies, 300 °C appears as a threshold: holding at 300 °C for extended time substantially reduces NBOHC PL/ESR [45]. At 400 °C, NBOHC annealing accelerates and is largely complete on the scale of minutes to hours. Annealing is strongly facilitated by hydrogen: NBOHC + H^+/H· → Si–OH, effectively erasing the hole center at or near room temperature if radiolytic H is present [22]. The activation energy for intrinsic NBOHC annealing is inferred to be relatively low (order ~0.8 eV), consistent with appreciable annealing at 200 °C [28]. Mechanistically, in dry silica NBOHC must capture an electron (often in tandem with an E′ annihilation) to reform bridging oxygen; in H-rich silica, H passivation dominates [22].

Peroxy Radicals and Oxygen-Related Defects

Peroxy radicals (≡Si–OO·) typically form during annealing (200–500 °C) when O_2 can diffuse to E′ sites [32]. The rate-limiting step is O_2 diffusion (activation ~1.0–1.4 eV in normal silica), matching the observed threshold around 200–300 °C [32]. Once formed, peroxy radicals are moderately stable; above ~500−600 °C they dissociate, releasing O_2 and restoring network bonds. Thus, O_2 provides an alternative annealing pathway: it "heals" a vacancy by filling it with O_2 (E′ → peroxy) and at higher T completes healing (peroxy → Si–O–Si + O_2).

Chlorine-Related Defect Annealing

Cl atom centers (Cl^0) are long-lived at room temperature; annealing generally requires >400 °C. At such T, Cl^0 can recombine ($2\,Cl^0 \rightarrow Cl_2$) or rebond with an E′ site (Si–Cl reformation). Efficient removal typically needs >500 °C; high-T anneals (~800–1000 °C) in O_2 can outgas Cl species and restore transparency [22]. For most natural aggregates (low Cl), these centers are minor.

5.4 DYNAMIC ANNEALING UNDER SIMULTANEOUS IRRADIATION AND HEATING

When gamma irradiation is applied while heating, defects can anneal as they form. At ~250–300 °C, radiolytic H_2 becomes mobile and reacts with E′ on the fly, suppressing net E′ accumulation; NBOHCs convert to silanols in situ. Thus, irradiating at elevated T yields lower steady-state E′/NBOHC densities and more end-products (Si–OH, Si–H, peroxy) [28]. Early studies noted temperature-dependent coloration/ESR yields consistent with concurrent annealing in both quartz and amorphous silica. In practice (e.g., fibers), hydrogen-loaded silica irradiated at elevated T shows reduced radiation-induced attenuation (RIA) and faster recovery due to ongoing reactions during exposure [22]. Dynamic annealing can also mitigate radiation-induced compaction by allowing structural relaxation during dose. For natural aggregates in reactors (50–80 °C), steady-state defect populations will be lower than RT predictions due to slow concurrent annealing.

5.5 SUMMARY OF GAMMA IRRADIATION EFFECTS

For amorphous silica (including natural aggregates), gamma-induced defects are not immutable: most E′ and NBOHC centers bleach between ~150–400 °C through reactions with $H_2/H_2O/O_2$ or by intrinsic recombination; maintaining samples warm during irradiation limits steady-state damage. Densification relaxes more slowly and may be incomplete. These conclusions are consistent across ESR/optical kinetics, IR chemistry, in situ irradiation/anneal experiments, and DFT/MD modeling [8, 27, 31][22][32][45][12][18][28]. Table 2 summarizes defect types, annealing ranges, and mechanisms related to gamma irradiation.

6. IRRADIATION CREEP IN AMORPHOUS SILICA (A-SiO_2)

Amorphous SiO_2 (silica glass) is normally a rigid, brittle material at room temperature ($T_g \approx 1373$ K), with negligible plastic deformation under stress. However, under energetic radiation, silica can undergo irradiation-induced creep—permanent deformation under stress facilitated by radiation—even at low temperatures (< 100 °C). This phenomenon, observed in nuclear materials, refers to stress-driven dimensional changes caused by continuous defect generation and structural rearrangements from irradiation. Below 100 °C (far below silica's T_g), thermal activation alone is insufficient for viscous flow, so any creep implies radiation-driven mechanisms. This section surveys experimental evidence and theoretical models for irradiation creep in a-SiO_2 at low temperature, covering different irradiation types (electron, gamma, neutron, ion) and sample scales (bulk vs. nanoscale). We discuss whether such creep is observed, the proposed mechanisms (e.g., defect-mediated flow, bond switching, thermal spikes), comparative behavior across radiation types and geometries, quantitative creep rates and defect production rates, and any threshold conditions for significant creep.

Table 2. Summary of defect types, annealing ranges, and mechanisms related to gamma irradiation

Defect Center	Description & Origin	Signatures (Detection)	Annealing Range	E_a (rep.)	Mechanisms
E′ (≡Si•)	Si dangling bond from Si–O rupture; intrinsic vacancy-like defect; often from strained rings / self-trapped excitation (STE) decay [22]	ESR $g \approx 2.001$; deep-UV band ~5.8 eV [22, 18]	Dry: start ~200–300°C; major loss 400–500°C; near-gone by ~600°C. With H_2/H_2O: partial RT decay; strong 100–300°C [27][31][45]	~2 eV (intrinsic, distrib.); 1.23 eV (E′+H_2O) [31]	Recomb. with NBOHC → Si–O–Si [31]; E′+H_2O → Si–OH + H• [31]; E′+H_2 → Si–H (H(I)) [22]; E′+O_2 → peroxy [32]
NBOHC (≡Si–O•)	Hole on non-bridging O; complementary to E′ from same bond break / STE decay [22]	ESR $g \approx 2.008$; 4.8 eV band; red PL ~1.9 eV [12][18]	RT decay if H present; dry: begins ~150–250°C; largely gone by 300–400°C [45]	~0.8–1.0 eV (inferred) [28]	Captures e^- → Si–O– Si (with E′ partner) [31]; H passivation: → Si–OH [22]
Peroxy radical (≡Si–OO•)	O_2 inserted at vacancy; annealed state of E′ in presence of O_2 [32]	ESR $g \sim 2.011$; UV band ~4.4–5.0 eV; O_2 (1272 nm) luminescence [22][32]	Forms ~200–450°C (O_2-diffusion limited); breaks down >500–600°C [32]	O_2 diffusion ~1.0–1.4 eV (glass-type dependent) [32]	E′+O_2 → peroxy; further anneal → Si–O–Si + O_2 ↑
H-related (H(I): Si–H; Silanol: Si–OH)	Extrinsic end-states from H reactions: E′+H_2 → Si–H; NBOHC+H → Si–OH [22][28]	ESR: H(I) hyperfine; IR: Si–H ~2260 cm^{-1}, Si–OH ~3670 cm^{-1}; H_2 consumption in IR [27][31][22]	H(I): decreases above ~300–500°C; Silanol condenses >600°C (two-OH dehydroxylation)	~0.4–0.5 eV (H_2 diff.) [28]; ~1.0–1.2 eV (OH condensation)	Si–H + Si–OH → Si–O–Si + H_2; Si–OH + Si–OH → Si–O–Si + H_2O; high-T outgassing
Cl-related (Cl^0, Cl_2)	Extrinsic in Cl-doped silica; γ breaks Si–Cl producing Cl^0 + E′ [22]	ESR: Cl^0 hyperfine; Optical: ~3.26 eV (Cl^0), ~3.78 eV (Cl_2^-) [22]	Little RT decay; recomb. begins ≳300–400°C; efficient removal >500°C; near restore >800°C	(High; diffusion-limited, ~1.5–2.0 eV effective)	2 Cl^0 → Cl_2 (trapped); Cl^0 + E′ → Si–Cl; high-T outgassing in O_2

6.1 EXPERIMENTAL OBSERVATIONS AT TEMPERATURES < 100 °C

Bulk Silica Under Irradiation and Stress

Early experiments on bulk silica and related glasses under stress and irradiation provided clear evidence of irradiation creep at ambient to moderate temperatures. For example, length-change tests on silica and borosilicate glass under applied tensile stress during 2 MeV proton and high-energy electron irradiation (up to 400 °C) showed an initial densification (compaction), followed by steady irradiation-induced creep with a linear stress dependence, characteristic of viscous flow [14]. Notably, UV photons (purely ionizing, low-energy) produced no dimensional change, whereas energetic protons and electrons did—indicating that radiation damage (atomic displacements) is required to induce deformation [14]. In these tests, after a transient compaction strain (which saturated at a few percent volume change), the glass continued to elongate under load at a constant creep rate proportional to both the radiation dose rate and the applied stress [14]. The creep compliance was essentially independent of temperature from room temperature up to ~400 °C [14]. Elevating the temperature mainly reduced the total compaction via annealing of defects, but the steady-state creep rate remained nearly constant [14].

This indicates that below 100 °C—in fact, across a broad sub-T_g range—creep in a-SiO_2 is controlled by irradiation effects rather than thermal activation. Pure crystalline SiO_2 (quartz) behaves differently: under the same proton irradiation, quartz showed a continuous irradiation-induced dilatation with very little stress-dependent strain, suggesting amorphous silica is far more susceptible to radiation creep [14]. In quartz, an upper bound on viscous compliance could only be estimated, whereas silica glass exhibited clear viscous flow under stress when irradiated [14].

Nanoscale and In Situ Experiments

Advances in microscopy have enabled direct observation of irradiation creep in small silica specimens at low temperature. In situ TEM mechanical tests show that a-SiO_2 undergoes creep under the electron beam itself, even at room temperature [46]. For instance, Zhang et al. (2023) performed bending tests on micron-scale silica beams inside a TEM: under the TEM's 200 keV electron beam, the silica samples exhibited measurable creep deformation at 25 °C [46]. By using digital image correlation and finite element modeling, they extracted creep constitutive parameters and found a linear relationship between creep strain rate and applied stress [46]. This implies a Newtonian (viscous) flow behavior induced by the electron irradiation, with an irradiation-dependent viscosity. Notably, such electron-beam-induced creep (sometimes termed electron-irradiation creep or radiation-assisted flow) is invariably present during in situ TEM mechanical tests on silica. It must therefore be accounted for, as the electron beam can significantly relax stress and cause time-dependent deformation even in nominally "static" experiments [46].

At the nanoscale, radiation can even enable superplastic-like deformation of silica at ambient conditions. Zheng et al. demonstrated dramatic shape changes in silica nanoparticles and nanowires under moderate-intensity electron beams in a TEM [47]. In situ tests showed that a low-current electron beam ($\sim 10^{-2}$ A cm^{-2}) allows large homogeneous strains in silica: for example, >200% tensile elongation in a 36 nm diameter silica nanowire at room temperature, without fracturing [47]. Under e-beam irradiation, the flow stress of silica nanostructures dropped by up to 4 times, and strain rates exceeding 10^{-4} s^{-1} were achieved close to RT [47]. In complementary experiments on ~500 nm silica particles, Zheng et al. observed similarly enhanced plasticity in compression: a particle could be flattened ("pancaked") under the e-beam with steady flow stress of only ~2.5 GPa [47]. With the beam off, significantly higher stresses

(approaching ~9 GPa in their setup) were required to achieve much smaller deformation, whereas with the beam on, the glass flowed smoothly without shear localization or cracking [47]. These in situ nano-scale experiments conclusively show that irradiation creep occurs in a-SiO_2 at low temperatures across length scales, from bulk samples down to nanostructures. The presence of a radiation field fundamentally changes silica's mechanical response, allowing time-dependent deformation under stresses that would normally cause immediate brittle failure.

Micropillar Heavy Ion Creep Tests

A series of micro-compression experiments by Özerinç et al. provided quantitative measures of irradiation creep in a-SiO_2 at room temperature [49]. In these tests, micropillars of silica (~2 μm in diameter and 2 μm tall) were subjected to uniaxial compressive stress while being bombarded in situ with MeV heavy ions (e.g., 2 MeV Kr^+). Displacement was measured with nanometer precision during irradiation, allowing direct calculation of strain rates. All tested amorphous materials, including silica, exhibited Newtonian (linear) creep under irradiation, meaning the strain rate $\dot{\varepsilon}$ was proportional to the applied stress σ (with no yield threshold observed) [49]. For 2 MeV Kr^+ ion irradiation of silica at ~25 °C, the irradiation-induced fluidity (defined as $\dot{\varepsilon}/(\sigma\dot{\Phi})$, where $\dot{\Phi}$ is the damage rate in dpa/s) was measured to be on the order of ~3 GPa^{-1} dpa^{-1} [49]. In other words, per unit stress and per unit of radiation damage (1 dpa), silica undergoes a shear strain on the order of 3 (dimensionless). This fluidity value is comparable to that observed in other amorphous materials, such as metallic glasses, under similar conditions [49].

Interestingly, when a lighter ion was used on silica in the same setup (2 MeV Ne^+), a much higher fluidity of ~83 GPa^{-1} dpa^{-1} was recorded—demonstrating that different irradiation conditions can drastically change the creep rate [49]. The authors attributed the baseline ~3 GPa^{-1} dpa^{-1} fluidity to point-defect-mediated plastic flow from nuclear collision cascades, whereas the anomalously high fluidity with Ne^+ was linked to the ion's higher electronic energy loss, which generated intense local thermal spikes (localized collision cascades with transient heating) that further enhanced stress relaxation [49].

These micropillar experiments confirm that bulk-like irradiation creep processes operate even in micro-scale volumes of a-SiO_2. Notably, the measured fluidities (on the order of 0.5–3 GPa^{-1} dpa^{-1} in various amorphous metals and ~3 in silica) are consistent with values from macroscopic stress-relaxation experiments and molecular dynamics (MD) simulations [14, 49]. This suggests little to no size effect in the fundamental creep mechanism: the small samples simply enable higher damage rates and facilitate in situ observation, without altering the intrinsic creep behavior.

Neutron and Gamma Irradiation

Direct experimental data on neutron-irradiation creep in pure silica at < 100 °C are sparse, since silica is not typically used as a structural component in reactors aside from insulators or optical fibers. However, by analogy with ion-irradiation results, fast neutrons (which create similar atomic displacement cascades) are expected to induce viscous flow in silica under stress as well. Neutron irradiation of vitreous silica is known to cause network compaction and defect generation akin to heavy-ion bombardment [7], even in the absence of stress. Thus, if an external load is applied, irradiation creep under neutron flux should occur.

In reactor experiments on ceramic materials (e.g., SiC composites), irradiation creep is observed even at low temperatures, driven by neutron-produced point defects that enable deformation under stress [11]. While specific quantitative data for silica under neutron flux and stress are limited, the phenomenon is

nonetheless highly likely to exist.

Gamma rays, which primarily cause ionization (and generate secondary electrons), can also produce defects in silica (e.g., E′ centers ≡Si·, oxygen vacancies, peroxy radicals). Although gamma-induced creep in silica has not been emphasized in the literature as much as charged-particle irradiation, it is expected that high-dose gamma irradiation would similarly facilitate slow stress relaxation through continuous bond-breaking. Devine and colleagues have noted that in silica's mixed ionic-covalent network, both ionizing radiations (such as gamma rays or electrons) and displacive radiations (ions, neutrons) produce significant defect populations and network modifications [5].

Therefore, all major forms of radiation can induce some creep in a-SiO_2 at low temperatures, although their efficiency varies (as discussed next). Generally, ion or neutron irradiation—which directly displaces atoms—tends to be more efficient per dose at inducing creep than purely ionizing radiation (gamma/electron), which mostly breaks bonds. However, intense electron beams have been shown to cause substantial creep if the flux is high enough.

6.2 MECHANISMS OF RADIATION-INDUCED CREEP IN SILICA

Multiple mechanisms have been proposed to explain how irradiation enables viscous or plastic deformation in amorphous silica well below its thermal glass transition. These mechanisms are not mutually exclusive and often act in parallel, depending on the type of radiation and energy deposition conditions.

Point-Defect-Mediated Viscous Flow

One widely supported mechanism is that radiation continually creates point defects in the glass (such as coordination defects, vacancies, and interstitials in the disordered network), which act as "flow defects" enabling local atomic rearrangements under stress. Molecular dynamics simulations by Mayr et al. (2003) on a model Cu–Ti metallic glass demonstrated that radiation-induced flow is governed by the production and migration of point-defect-like entities [26]. Notably, their simulations showed that the amount of flow per defect was independent of the primary knock-on atom's energy in the range ~0.1–10 keV, when compared on the basis of an equal number of defects produced. In other words, it is the number of radiation-produced defects (not the kinetic energy per se) that controls the strain [26]. They also identified a threshold recoil energy of approximately ~10 eV to induce any permanent flow in the glass—essentially corresponding to the minimum energy required to displace an atom and create a stable defect [26]. Once defects are created, the simulations showed that even at 10 K, the glass yielded a similar amount of flow per defect as at higher temperatures, indicating that thermal activation is not required for these defect-mediated plastic events [26]. Instead, radiation-produced defects (e.g., under-coordinated Si or O atoms, broken Si–O bonds) locally lower the energy barriers for structural rearrangement. Under an applied stress, these defective regions can deform (e.g., by atoms rearranging or "dissolving" into open volume), and subsequent recombination or annealing of the defects leaves a net strain increment. Essentially, radiation continuously generates a population of weak sites that undergo biased rearrangements, enabling steady-state creep at a rate proportional to the defect production rate (i.e., proportional to dose rate). This point-defect viscous flow model can quantitatively explain the moderate irradiation creep rates observed in experiments. For instance, the fluidity ~3 GPa^{-1} dpa^{-1} measured for heavy-ion-irradiated silica [49] corresponds well to predictions assuming each displacement cascade produces a certain number of flow defects that relax the stress field. In silica, specific defect structures such as E′ centers (≡Si·, a dangling bond on Si) and oxygen vacancies, or other strained bond configurations, may serve as these flow units.

The fact that silica's irradiation creep rate was nearly constant from ~$0.1T_g$ to $0.4T_g$ [26] in experiments supports a defect-driven athermal mechanism, since thermal diffusion of defects is minimal at such low temperatures. In summary, the continuous creation and (eventual) annihilation of point defects under stress lead to a viscous-like deformation of the amorphous network without the need for thermal activation.

Bond Switching and Network Rearrangement

On the atomic scale, radiation can induce bond breaking and bond switching events that facilitate plastic flow. In a covalent network glass like SiO_2, plastic deformation (even near T_g) is known to proceed by the breaking of Si–O bonds and reforming them in new configurations ("network restructuring"). Under irradiation, energetic particles or photons break Si–O bonds, creating unsaturated dangling bonds (e.g., a 3-coordinated Si and a non-bridging O) that can subsequently re-bind in different topologies. This is effectively a dynamic rearrangement mechanism: the rigid SiO_2 tetrahedral network is temporarily opened at a bond, allowing local atomic clusters to rotate or slide under stress, then a new bond forms in a configuration that accommodates the deformation. Radiation essentially bypasses the thermal activation needed for bond switching by directly depositing energy into the bonds. For example, electron-beam studies propose that silica-s viscous flow is driven largely by bond-switching: broken siloxane bonds (≡Si–O–Si≡) create mobile units that enable flow until they re-connect [3, 15]. Zheng et al. observed that under stress, bond breaking/switching mediates the rotation and translation of atomic clusters in silica; the electron beam continuously produces oxygen vacancies and dangling bonds throughout the material, sustaining a high density of these "flow-enabling" sites [47]. Thus, irradiation lowers the viscosity by constantly generating broken-bond configurations, analogous to increasing the number of fluid-like defects. This mechanism aligns with the point-defect picture but emphasizes the specific role of bond rupture and reformation. Direct experimental evidence comes from observations that electron-irradiated silica can deform homogeneously without crystallization (no signs of nanocrystallite formation), and that the defect population (measured by EPR or optical spectroscopy) correlates with the degree of plastic strain. In essence, radiation provides a non-thermal activation pathway for bond switching, causing a-SiO_2 to behave like a viscous liquid under stress even at room temperature.

Thermal Spike (Localized Melting) Mechanism

For high-energy ion or neutron irradiation, a significant portion of the energy goes into dense collision cascades that create concentrated defect clusters and intense local heating—known as thermal spikes. In silica, a thermal spike can momentarily heat a nanometer-sized region to a high temperature (potentially approaching or exceeding T_g) for a few picoseconds. During this brief period, the local region becomes fluid-like and can undergo stress-driven flow (shear or expansion) before rapidly quenching back to the glassy state. Trinkaus [39, 41] developed a thermal spike model to explain irradiation creep of amorphous solids. The model posits that local stress is relaxed in the transient molten cores of collision cascades, and when the region re-solidifies, the material freezes in the deformed configuration, producing a permanent strain increment [39, 41]. This process repeats for each cascade, yielding a creep strain that accumulates linearly with dose (since each cascade contributes an incremental strain). Importantly, the thermal spike mechanism is most relevant for heavier ions or energetic recoils that deposit high energy densities in collisions. Trinkaus showed that experimental data for MeV medium and heavy ions irradiating vitreous silica could be explained by thermal spike-induced viscous flow [39, 41]. Under those conditions, cascades produce a quasi-molten zone, and an applied stress biases the flow of material out of that zone (similar to squeezing a droplet) before it refreezes [39, 41]. The model predicted a linear creep rate vs. stress and dose

rate, consistent with observations, with the magnitude of creep strongly tied to the cascade energy. In contrast, for lighter irradiating particles (protons, electrons, or very light ions), full thermal spikes may not develop; instead, electronic excitations and point-defect mechanisms dominate (as discussed before). In fact, Trinkaus noted that for 6 MeV proton irradiation of silica, electronic excitation effects had to be included to explain the measured viscous flow—meaning that ionization alone (without significant thermal spike heating) can also induce creep, via the bond-switching or radiolysis-mediated processes [39, 41]. Nonetheless, whenever the electronic energy loss of ions exceeds a threshold (on the order of ~1 keV/nm in silica), thermal spike contributions become significant, enhancing the creep rate. This explains the micropillar result that 2 MeV Ne^+ (which has a higher fraction of its energy going into ionization) produced ~25× higher fluidity than Kr^+: Ne's smaller mass and higher velocity led to more energy being deposited into electronic excitation along its path, effectively generating spike-like conditions or extensive ionization-induced flow in the silica. In summary, the thermal spike mechanism is a special case of radiation creep where transient local melting under stress yields plastic deformation. It complements the defect/bond-switching mechanisms; in silica, it likely operates concurrently under heavy-ion or high-flux neutron irradiation, especially when dense cascades overlap at high fluence.

Radiolytic Compaction and Creep Interplay

It is worth noting that radiation causes macroscopic volume changes in silica (even without external stress) which can interplay with creep. At low to moderate doses, a-SiO_2 typically undergoes compaction (density increase of ~1–3%) due to irradiation-induced structural tightening and collapse of free volume [14]. At very high doses or under certain high ionization conditions, swelling or microvoid formation can occur instead (e.g., in highly damaged or micro-porous silica) [14]. These volumetric changes can be thought of as creep under a hydrostatic or zero-stress condition. Under uniaxial stress, the same processes that cause isotropic compaction can instead contribute to anisotropic creep strain in the loading direction. For example, the creation of smaller ring structures and more acute Si–O–Si bond angles (as observed in irradiated silica networks [14, 6]) leads to a denser structure; if no external stress is applied, the sample shrinks uniformly, but if a tensile stress is present, the network may preferentially contract laterally (perpendicular to the tensile axis) and elongate along the stress axis, manifesting as creep strain. Thus, irradiation creep and densification are coupled: initial radiation damage usually causes compaction in all directions until certain defects saturate, after which continued irradiation under stress produces primarily deviatoric strain (creep) with little further volume change [14]. Experiments confirm that once the asymptotic compaction strain is reached, further dose yields steady creep without additional volume change [14]. The independence of creep rate from the total prior compaction suggests that after the network's free volume and weak bonds are exhausted by early damage, the ongoing creep is controlled by the continuous creation of new defects (not by any remaining free volume). One can view compaction as arising from predominantly shrinkage-type bond rearrangements (ring collapse, bond angle relaxation) and creep as arising from shear-type rearrangements—but both ultimately are driven by radiation-generated defects and bond switches under the appropriate stress conditions.

In summary, irradiation lowers the resistance to flow in silica via two primary avenues: (1) continuous generation of point defects and broken bonds (via atomic displacements or ionization) that enable stress-biased viscous flow; and (2) intense local energy deposition in collision cascades (thermal spikes) that momentarily fluidize regions under stress. Both result in a Newtonian creep behavior—a steady strain rate proportional to stress and dose rate—even at temperatures where thermal creep is negligible.

6.3 COMPARISON ACROSS IRRADIATION TYPES

Different radiation types impact silica's creep behavior through the nature of energy deposition (displacive vs. ionizing) and the distribution of damage they produce:

Heavy Ions (e.g., MeV Kr, Au)

These produce dense collision cascades with significant local defect production and spike heating. Silica under heavy-ion bombardment exhibits pronounced irradiation creep and even spontaneous anisotropic shape changes. A free-standing glass can elongate in the beam direction under heavy-ion irradiation even without external stress—a phenomenon known as ion hammering. Under an applied load, heavy ions effectively accelerate creep by constantly "stirring" the structure via collision cascades [14, 49]. The thermal spike mechanism applies strongly here: medium-to-heavy ions in the MeV range induce viscous flow consistent with stress relaxation in collision cascades [14, 49]. Notably, heavy-ion-induced creep tends to be relatively insensitive to the absolute dose rate beyond the basic linear proportionality (since each cascade contributes a fixed strain increment per dpa). There is no clear threshold fluence for onset; measurable creep begins as soon as damage is produced. However, above certain electronic stopping powers (~1 keV/nm in silica), heavy ions cause even larger fluidities, implying a transition to a mixed defect+spike regime [14, 49]. In practical terms, a silica glass under a heavy ion beam (such as used in ion irradiation facilities) will creep at a rate set by the ion flux (dpa/s) and the applied stress—with higher ion energies or heavier ion species generally yielding more damage per ion (and thus more creep per ion), up to the point where electronic energy losses start to dominate the process.

Light Ions, Protons, α

Lighter ions primarily cause sparse, isolated collision events and significant ionization along their tracks. For example, 6.2 MeV protons in silica produce relatively few direct atomic displacements but a large number of electronic excitations. Proton irradiation experiments show that silica still creeps linearly with dose, but in this case the mechanism relies more on radiolytic bond breaking and electronic excitation rather than thermal spikes [49]. Light ions can thus induce creep, but the efficiency (strain per dpa) may differ. Özerinç's data for 2 MeV Ne^+ vs. Kr^+ is illustrative: Ne (a lighter ion) caused a much higher creep strain per dpa in silica than Kr, because Ne's higher velocity (and lower mass) meant that a larger fraction of its energy was lost to electronic ionization, which in silica triggered additional fluidization (via localized electronic "heating" or enhanced bond-breakage) [14, 49]. This suggests that for highly ionizing radiation, silica is extremely susceptible to radiation-assisted flow.

In contrast, very low-energy light ions (e.g., keV He^+ implants) produce mostly isolated point defects. Silica would still creep, but at lower rates, because the defect production per ion is low and no significant thermal spikes occur. Overall, all ions (light or heavy) cause some irradiation creep in silica at low temperatures, but the damage morphology (diffuse point defects vs. overlapping cascades) influences the dominant mechanism (defect-mediated vs. spike-mediated) and thus the quantitative creep rate.

Neutron Irradiation

Fast neutrons impart recoil energies to atoms similar to those of medium-heavy ions (tens of keV), but the damage is distributed uniformly throughout bulk samples (due to the high penetration of neutrons). In nuclear reactor conditions (a neutron flux accompanied by concurrent gamma radiation), silica insulators or

components experience significant displacement damage over time. Neutron-irradiation creep in amorphous ceramics has been documented; for instance, silicon carbide (SiC) fibers exhibit creep under neutron flux at stresses and temperatures where no thermal creep would occur [16]. By analogy, a neutron-irradiated silica glass under load should undergo creep via the same point-defect and cascade mechanisms described earlier. Each fast neutron collision cascade in silica will produce local defects and possibly a small thermal spike. Because neutrons penetrate deeply, a bulk silica component can undergo uniform creep throughout its volume (rather than just a surface layer, as is the case for ion beams of limited range). If a silica sample were under load in a reactor, one would expect a linear strain accumulation with neutron fluence. One difference is that neutrons have a broad energy spectrum: high-energy neutrons create dense cascades (like heavy ions), while intermediate-energy neutrons can also cause nuclear reactions (e.g., (n,α) reactions) that produce helium atoms and extra damage. Helium accumulation could influence creep by inducing volumetric swelling or bubble formation at very high doses, although at $< 100\,^{\circ}\mathrm{C}$ the mobility of He and growth of bubbles is very limited. In summary, neutrons should induce irradiation creep comparable to ion bombardment of an equivalent dpa, with both point defects and thermal spikes contributing. No specific threshold neutron flux is needed—as soon as neutrons create a flux of freely migrating defects, creep will begin (linearly with dose rate) [44]. A practical consideration is that neutron creep experiments on silica are challenging and rare, so our understanding relies on theory and indirect evidence. But given that reactor core metals and ceramics show irradiation creep from neutron damage [11], the amorphous network of silica—which deforms even more readily under radiation—certainly would as well at low temperature.

Electron and Gamma Irradiation

Purely ionizing radiation (high-energy electrons, X-rays, gamma rays) interacts with silica primarily by ejecting electrons from atoms (ionization), breaking bonds (radiolysis), and causing charge accumulation. Does such radiation cause creep? The evidence indicates that it does, although high dose rates or intense beams are typically required. High-voltage electron microscope (HVEM) irradiations of silica-based glasses, for example, can cause significant defect accumulation (one HVEM study drove a nuclear waste glass to ~2.5 dpa using 1 MeV electrons, resulting in void formation and other microstructural changes [14]). Under stress, such defect buildup would translate to creep strain. Recent in situ TEM work confirmed that even the $\sim 10^{7}$–$10^{8}\,\mathrm{Gy\,s^{-1}}$ localized dose rate of a 200 keV electron beam in a TEM can induce steady creep in silica at $25\,^{\circ}\mathrm{C}$ [46].

Mechanistically, electrons primarily produce isolated bond breaks and induce trapped charges in the network. Recent research increasingly suggests that injected electrons and the resulting internal charge accumulation are governing factors for the relaxation and deformation of silica under e-beam irradiation [36]. Bombarding silica with electrons creates a cloud of negative charge inside; this can weaken bonds (through electrostatic repulsion or alteration of the local potential energy landscape) and promote bond-switching events, thereby enhancing flow. If the electron flux is high enough, the continuous generation of dangling bonds (≡Si· and ≡Si–O·) and peroxy linkages (≡Si–O–O–Si≡) keeps the glass in a continuously damaged, deformable state, where it responds viscously even to small stresses.

Gamma rays similarly deposit energy by ionizing the material and producing energetic electrons throughout the volume. While gamma-induced creep in silica has not been separately quantified in the literature (since gamma irradiation of glass is often studied without applied stress), it is known that gamma irradiation produces defects of the same kind (E′ centers, non-bridging oxygens, etc.) as electron beams

[14]. Therefore, under load, gamma-irradiated silica would be expected to creep, although likely at a slower rate than an equivalent dpa from neutrons or ions, since gamma rays are inefficient at displacing atoms (most gamma energy goes into ionization, and each ionization event yields only minor structural adjustments unless the dose rate is extremely high).

In nuclear waste storage scenarios, long-term gamma exposure is considered as a factor in glass dimensional stability, but the dominant effect at $< 100\,^{\circ}\mathrm{C}$ is usually compaction (volume shrinkage) rather than creep because these glasses are not typically under stress. If stress were present, the network's tendency to contract under radiation could indeed manifest as creep strain.

In summary, electron beams (hundreds of keV) have been directly shown to induce creep in a-SiO_2, and, by extension, sufficiently high-dose gamma irradiation (which generates energetic electrons within the material) should do the same—albeit requiring significant total doses to accumulate appreciable strain. The creep mechanism for purely ionizing radiation is primarily via radiolysis-driven bond switching and defect creation, rather than thermal spikes.

6.4 QUANTITATIVE DATA AND THRESHOLD CONDITIONS

Creep Rates and Fluidities: As compiled above, a-SiO_2 under irradiation at $< 100\,^{\circ}\mathrm{C}$ exhibits Newtonian creep with a strain rate typically on the order of 10^{-10}–$10^{-8}\ \mathrm{s}^{-1}$ under typical reactor-level fluxes and stresses, up to $\sim 10^{-3}\ \mathrm{s}^{-1}$ under extreme laboratory conditions. A convenient metric is the irradiation creep compliance, often given in units of (Pa^{-1} per dpa/s) or simply $\mathrm{GPa}^{-1}\ \mathrm{dpa}^{-1}$ (the fluidity). For silica at room temperature, measured values include $\sim 3\ \mathrm{GPa}^{-1}\ \mathrm{dpa}^{-1}$ for heavy-ion irradiation (nuclear collision dominated), rising to tens of $\mathrm{GPa}^{-1}\ \mathrm{dpa}^{-1}$ when electronic stopping or radiolysis dominates (e.g., 83 for Ne ions, and similarly high for intense electron beams) [14]. In one study, silica's creep compliance under combined electron/proton irradiation was on the order of 10^{-5}–10^{-4} per (MPa·dpa) (after converting units), essentially aligning with the above fluidity range [14]. By comparison, metallic glasses have similar fluidities ($\sim$1–5 $\mathrm{GPa}^{-1}\ \mathrm{dpa}^{-1}$) [14], whereas crystalline materials (metals, SiC) have much lower irradiation creep compliances (orders of magnitude lower strain per dpa) under comparable conditions. The implication is that amorphous silica is among the more creep-sensitive materials under irradiation.

To put numbers in perspective: consider a silica component under a stress of 100 MPa and a damage rate of 10^{-7} dpa/s (a plausible high neutron flux in a reactor). Using a fluidity of $\sim 3\ \mathrm{GPa}^{-1}\ \mathrm{dpa}^{-1}$, the creep strain rate would be $\dot{\varepsilon} \approx 3 \times (100\ \mathrm{MPa})^{-1} \times 10^{-7}\ \mathrm{s}^{-1} \approx 3 \times 10^{-10}\ \mathrm{s}^{-1}$. This corresponds to on the order of $\sim$1% strain per year. If the dose rate is higher, say 10^{-4} dpa/s (achievable in a dedicated ion beam) and stress ~ 0.5 GPa (as in the micropillar tests), $\dot{\varepsilon}$ could reach $\sim 10^{-5}\ \mathrm{s}^{-1}$ (on the order of 0.1% strain per second). Under the extreme conditions of nanowire experiments—an estimated dose rate equivalent to $\sim 10^{8}$ Gy/s (from the electron beam) and an effective stress approaching 1 GPa—strain rates in the range of 10^{-4}–$10^{-3}\ \mathrm{s}^{-1}$ were observed [47]. Thus, under very high radiation flux and stress, silica can deform almost like a viscous liquid. Under more realistic radiation environments (e.g., 10^{-7}–10^{-8} dpa/s in reactor components) and modest stresses, creep strains will accumulate slowly over months to years—but do so orders of magnitude faster still than thermal creep at $< 100\,^{\circ}\mathrm{C}$ (which is essentially zero on such timescales).

Bulk vs. Nanoscale Geometry Effects: While the fundamental irradiation creep mechanisms appear intrinsic to the amorphous structure and do not depend on sample size, there are practical differences when comparing bulk vs. microscale silica. One is the magnitude of achievable strain before failure. Bulk silica components (macroscopic) usually fracture at very small strains if stressed without irradiation, being

brittle. Under irradiation, they can deform more before failure, but still, a bulk sample may crack after only a few percent tensile strain (especially if irradiation induces local heterogeneities). In contrast, nanoscale silica (fibers, particles, pillars) under irradiation can sustain extremely large homogeneous strains (tens to even hundreds of percent) [47]. This is partly because smaller samples have fewer pre-existing flaws and because radiation can activate flow uniformly across the small volume. The nature of irradiation creep—distributed throughout the material—means that in a tiny sample, the entire gauge length is deforming, allowing very high ductility. For example, the silica nanowire in [47] elongated >200% before thinning out, something a bulk rod could never approach (it would crack well before that strain). Thus, nanoscale samples can exhibit "superplastic" irradiation creep, whereas bulk samples might be limited to a few percent strain before fracturing (though in compression, bulk silica could possibly accumulate more strain without failing due to the absence of tensile cracking).

Another consideration is **surface effects and stress state**. In micropillars or thin specimens, free surfaces may allow radiation-induced point defects to escape or recombine more readily, potentially reducing the steady-state damage accumulation. However, experiments showed that silica micropillar creep rates were consistent with bulk values, suggesting surface sink effects are minor compared to the overall defect generation rate [49]. On the other hand, free surfaces in nano-samples can relieve triaxial stress states, enabling more uniform deformation. Bulk samples under tension might experience localized necking or internal stress concentrations that could interact with radiation defects (e.g., preferential void growth sites). At the small scale, stress is often essentially uniaxial and homogeneous, aligning with the ideal conditions assumed in models (uniform stress + uniform irradiation = uniform creep).

Dose uniformity is another difference. In bulk irradiation (e.g., neutrons or gammas in a reactor, or ions penetrating a thick sample), the dose may be non-uniform (due to attenuation with depth or the finite range of ions). This can lead to gradients in creep strain or bending of components. In microscale samples (like a $\sim 1\,\mu$m pillar), many MeV ion beams can uniformly irradiate through the thickness, and electron beams easily penetrate such small volumes, yielding a uniform damage profile. This uniformity helps achieve steady, homogeneous creep. In a thick bulk sample, by contrast, only a surface layer may be heavily irradiated (and creeping) while the interior remains undeformed, potentially causing additional bending or shape distortions.

Finally, **experimental measurement** is easier on small scales. Intense irradiation can produce measurable strain in a microscale sample within minutes (as in in situ TEM or ion beam tests), whereas detecting a similar creep strain in a bulk sample at low temperature might require many hours or days of irradiation. Bulk low-temperature creep tests thus demand either very sensitive displacement measurements (e.g., laser interferometry) or extended irradiation times, which historically made them challenging. This is one reason definitive evidence for silica's irradiation creep emerged relatively late (1990s–2000s) compared to metals—it required either high-dose accelerators or in situ techniques. Now, with micropillar methods and TEM, one can directly watch a tiny silica sample creep in real time. These techniques have confirmed that the underlying creep behavior is the same: linear in stress and dose, with comparable fluidity values, whether in a micron-scale pillar or extrapolated to bulk [14].

In conclusion, geometry mainly influences how the creep manifests (e.g., the extent of strain before failure, or the ease of observing it), but not whether it occurs. Amorphous silica shows irradiation creep from the nano- to macro-scale. If anything, smaller scales enable more dramatic demonstrations of the effect—because high stresses and dose rates can be applied without destroying the sample, and the material's uniformity is maintained. Bulk silica under load in a radiation field will creep too, but practical

limits (e.g., early failure or non-uniform irradiation) may cap the observable strain in those cases.

Thresholds: Experiments consistently find no apparent threshold stress for the onset of irradiation creep in amorphous materials—the strain rate vs. stress relationship is linear and passes through the origin (within experimental resolution) [14]. Even a very small stress will bias defect-induced motions slightly and produce some creep (though below the detection limit, this is mostly of academic interest). In silica's case, the linear viscous behavior holds until extremely high stresses where other effects (densification-induced hardening or sample fracture) may intervene [14]. There is effectively no yield stress for radiation-induced flow in silica in the regime studied; even at a few MPa of stress, given sufficient dose, creep will accumulate. By contrast, crystalline quartz under the same low stresses showed virtually no creep, highlighting how the amorphous structure enables radiation creep whereas the crystalline structure does not [14].

There is also no strict threshold dose for creep, but there is an initial transient when irradiation begins. Silica first undergoes compaction (densification) up to a saturation level (often ~0.1–0.2 dpa for vitreous silica, corresponding to ~2–3% volume change) [14], then the deformation under stress transitions to a steady-state creep. Beyond this saturation of compaction, each incremental radiation dose yields proportional strain (with no further significant volume change). Below that dose (early in irradiation), creep may be slightly less efficient because some fraction of the defects are still going into tightening the structure isotropically rather than shear deformation. Nonetheless, even during the initial 0–0.1 dpa, if stress is present, some creep strain will accumulate alongside compaction—it just reaches its full steady-state efficiency once the network's free volume is adjusted by the initial damage. Thus, from a practical standpoint, any non-zero dose rate will eventually produce creep; there is no abrupt dose threshold, though the creep rate ramps up as damage builds to the steady-state level.

The temperature threshold for irradiation creep is also effectively non-existent in the low-to-moderate temperature range. As noted, experiments showed virtually no change in silica's irradiation creep rate from room temperature up to ~100 °C and even to a few hundred °C [14, 49]. Up to ~0.3–0.4T_g (~400–500 °C for silica), the fluidity varies by less than about 50% [49]. Only at higher temperatures would one expect substantial changes: on one hand, thermal annealing of radiation defects becomes significant (reducing the net defect concentration for a given dose rate), and on the other, the glass itself approaches its glass transition and can creep thermally. In the context of < 100 °C, we can consider the irradiation creep rate to be entirely athermal and temperature-invariant—essentially governed by the radiation alone. MD simulations support this, showing that even at cryogenic temperatures (tens of K), displacement cascades in silica produce flow defects that induce plastic strain [26]. In summary, up to a few hundred degrees Celsius, silica's irradiation creep is controlled by radiation processes and is largely decoupled from temperature (except insofar as higher temperature might slightly reduce defect steady-state density by annealing) [14].

Finally, we note a special threshold relevant to very high-energy ions: the electronic energy loss threshold for ion track formation (in silica, a stopping power of ~5 keV/nm is cited) [40]. Swift heavy ions (GeV energies) can produce continuous latent tracks of damage in silica, causing anisotropic expansion along each ion path. Under stress, such tracks would effectively produce an elongation bias and could contribute to creep in a different manner (each ion leaving a stretched cylinder in the material) [40]. However, this regime of track-forming irradiations is typically encountered with cosmic rays or specialized accelerators, not in standard reactor or lab conditions. It serves as a reminder that at extreme energy depositions, additional modes of radiation creep (via track-induced deformation) can arise, but for most low-temperature applications the discussed mechanisms (point defects, bond switching, thermal spikes) dominate.

6.5 SUMMARY OF IRRADIATION CREEP OBSERVATIONS

In summary, amorphous SiO_2 exhibits irradiation creep at temperatures well below 100 °C, as demonstrated by multiple lines of research. Under concurrent radiation and stress, silica glass deforms in a time-dependent, viscous manner despite the lack of thermal activation. The creep arises from radiation-induced defects and structural transformations that enable the network to continuously rearrange under load. Key mechanisms include the generation and motion of point defects (vacancies, interstitials, dangling bonds) that act as "flow units," bond breakage and re-bonding (bond switching) that lubricates the network, and localized thermal spikes in collision cascades that transiently melt regions and allow stress relaxation.

Comparing irradiation types, we find that all forms of energetic radiation (ions, neutrons, electrons, gamma rays) can produce the requisite damage to cause creep in silica, although their efficiencies differ. Heavy ions and fast neutrons, through collision cascades, produce direct atomic displacements and sometimes thermal spikes, leading to substantial creep compliance that is largely athermal and high per dose. Electron and gamma irradiation rely on ionization damage and tend to induce creep more slowly, unless applied at very high flux; nonetheless, even electron beams in electron microscopes can provoke notable creep in silica at room temperature.

The unifying observation is a Newtonian creep law for amorphous silica under irradiation:

$$\dot{\varepsilon} = B\,\sigma\,\dot{\Phi},$$

where $\dot{\Phi}$ is the radiation dose rate and B is an irradiation-dependent fluidity (with units of Pa per dose rate). Quantitatively, experiments give fluidities on the order of 10^{-9} Pa^{-1} per (dpa/s) in silica when displacement damage dominates, up to $\sim 10^{-7}$ Pa^{-1} per (dpa/s) when ionization effects dominate [14]. These translate to significant strain rates under typical radiation fluxes.

There appear to be no sharp thresholds in stress or dose for the onset of irradiation creep in a-SiO_2. Even the slightest stress will induce some biased deformation once radiation generates defects, and even the first few atomic displacements contribute to strain. The "thresholds" are rather continuous transitions: e.g., the dose to reach damage saturation (after which steady-state creep prevails) and the energy loss level where thermal spikes start to enhance the creep. Temperature is not a limiting factor up to a few hundred °C—low-temperature irradiation creep is effective and largely constant in that regime [14, 49].

Finally, the behavior is consistent across scales: bulk silica can creep under irradiation (albeit only a modest total strain before failure), while micro/nanoscale silica can sustain dramatic plastic flow under irradiation (a fact exploited in nanofabrication techniques). This knowledge is crucial for applications ranging from the dimensional stability of silica-based nuclear waste glasses and fiber optics in radiation environments, to the deliberate use of electron beams to shape micro- and nanoscale silica devices. The literature consensus is that amorphous silica, normally locked in a brittle state at low T, becomes pliable under the influence of radiation—essentially undergoing a radiation-induced glass transition that allows stress-driven viscous deformation far below the thermal glass transition temperature.

7. SUMMARY OF ORIGINS OF FLUX EFFECTS

Experimental results demonstrate that neutron flux rate significantly impacts radiation-induced volumetric expansion (RIVE). Higher flux rates result in greater expansion compared to lower flux rates at identical total fluence.

RIVE varies across different concrete aggregate minerals and rocks based on their chemistry, formation, and internal structure. Quartz shows the largest swelling (15–18%) during crystalline-to-amorphous transformation, with flux strongly controlling defect recombination: low flux permits relaxation and reduces swelling, whereas high flux accelerates amorphization and expansion. Feldspar and granite also swell significantly due to their rigid polymerized silicate frameworks, and in granite differential swelling between phases generates internal stresses; again, low flux mitigates while high flux amplifies damage. Basalt and other mafic aggregates are less prone to swelling because of their less polymerized structures, though grain boundaries serve as defect sinks at low flux and microcracking emerges under high flux. Mica exhibits anisotropic swelling with early degradation, and amphibole shows intermediate behavior, both governed by flux such that low flux enables defect annealing and stress relaxation, while high flux leads to rapid defect buildup and structural instability.

Fundamentally, the main hypothesis being proposed here is that at the same total neutron fluence, the longer time associated with the lower flux enables more concurrent healing of irradiation-induced damage regardless of the dependence of specific healing mechanisms on flux. Accompanying gamma radiation and irradiation creep are also expected to play flux- and/or time-dependent roles in the healing process.

Various healing mechanisms are presented in this report and are summarized as follows.

- **Point defect recombination and migration:** Even below 100°C, some interstitial–vacancy pairs in quartz can recombine because certain defects retain limited mobility, may utilize quantum tunneling, or interact with lattice strain fields. Experiments confirm that paramagnetic centers in quartz diminish during room-temperature storage or mild annealing, indicating slow recombination. At low flux, defects have time to meet and annihilate (or be chemically terminated by OH impurities) before being frozen into the amorphous state. At high flux, successive collisions occur more rapidly such that recombination is more limited or reduced, leading to higher steady-state defect populations.
- **Structural relaxation of the amorphous network:** When quartz is partially amorphized, the disordered SiO_2 network can slowly relax or compact even at modest temperatures (room temperature to ~60–90°C). Ion irradiation studies have identified a very low activation energy process (~0.13 eV) linked to viscous flow or bond rearrangements in the amorphous structure. This gradual relaxation reduces internal stresses and can slightly densify amorphous pockets, counteracting swelling. At low flux, this relaxation has time to proceed between irradiation events. At high flux, ongoing bombardment interrupts the process and produces damage faster than it can be healed, increasing overall RIVE.
- **Cascade-induced annealing (thermal spikes):** Each fast neutron impact generates a short-lived, nanometer-scale thermal spike (10^4–10^5 K for a few picoseconds), which transiently melts and quenches the local network. This process can reorient Si–O tetrahedra and accommodate displaced atoms without forming permanent voids, effectively acting as instantaneous self-annealing. At low flux, cascades occur in largely relaxed regions, so each thermal spike contributes to gradual, distributed healing. At high flux, cascades strike regions that are still in metastable disordered states, which prevents them from achieving enough healing.

- **Delayed amorphization threshold (fluence dependence):** Because of the above recovery processes, the critical dose for quartz amorphization could be higher at low flux, even at < 100°C. In effect, time may substitute for temperature where slow irradiation may allow defects to recombine or relax between events, raising the fluence required for amorphization. At high flux, recovery is overwhelmed, the amorphous transition occurs more rapidly, and swelling is amplified. This flux effect mimics the role of higher irradiation temperature, which also shifts amorphization onset to higher doses by enabling defect annealing.

The literature review also found that gamma irradiation can further affect both defect formation and healing as follows:

Key Defects: Gamma irradiation induces intrinsic defects (E′ centers, non-bridging oxygen hole centers—NBOHCs) and extrinsic phenomena influenced by impurities (e.g., H, OH, Cl).

Possible annealing mechanisms:

- **Below** 100°**C**: Annealing at low temperatures is mainly chemically assisted, dominated by reactions with radiolytic hydrogen species. E′ centers can be passivated through reactions with H or H_2, forming Si–H bonds, while NBOHCs capture hydrogen to convert into stable silanols (Si–OH). Even during irradiation, dynamic annealing operates around 50–80°C, continuously reducing the steady-state concentration of E′ and NBOHC defects compared to room-temperature or cryogenic conditions. In dry silica without available $H/H_2/H_2O/O_2$, however, purely intrinsic thermal recombination remains negligible at these temperatures.
- **Above** 100°**C**: At higher temperatures, thermal pathways become more significant, complementing or surpassing chemical passivation. E′ and NBOHC centers begin to anneal intrinsically by recombination, while water-assisted processes ($E' + H_2O \rightarrow$ Si–OH + $H^{\cdot}$) become efficient in the 150–300°C range. Oxygen diffusion allows E′ centers to form peroxy radicals (≡Si–$OO^{\cdot}$) around 200–450°C, which subsequently anneal out above ~500°C. Meanwhile, hydrogen-related end products such as Si–H and Si–OH gradually diminish through dehydrogenation and dehydroxylation above 300–600°C, and chlorine-related color centers (if present) require similarly high temperatures (>400°C) for effective annealing.

Finally, irradiation-induced creep can also play an important role within the amortised silica as follows:

- **Irradiation creep occurs well below** 100 °C**, even without thermal activation.** Radiation-induced defects (vacancies, interstitials, dangling bonds) and bond-switching events act as "flow units," whereas local collision–cascade spikes transiently melt regions, enabling stress relaxation and time-dependent deformation under load.
- **All energetic radiation types can induce creep at low temperature, though efficiencies vary.** Heavy ions and fast neutrons (via collision cascades and thermal spikes) cause strong athermal creep per dose. Electron and gamma irradiation, driven mainly by ionization, induce creep more slowly but still measurably at room temperature, especially at high flux (e.g., in electron microscopy).

8. ION IRRADIATION AS A MEANS TO INVESTIGATE THE INTERPLAY BETWEEN NEUTRON AND GAMMA RADIATION

As has been presented in the previous sections, gamma irradiation may have a role in the observed overall RIVE. As listed in Table 1, there is a significant difference between the ratios of gamma and neutron doses for the different reactors. In this section, we present a preliminary computational study to investigate such neutron/gamma interplay using ion irradiation as a surrogate. Since ions are charged particles, their interaction with matter involves ballistic interactions (nuclear) and ionizing (electronic) interactions. Thus, qualitatively, nuclear interaction of ions could be considered a surrogate for neutron interaction, and electronic interaction of ions could be considered a surrogate for gamma interaction. By studying different ion-irradiated experiments and evaluating the electronic-to-nuclear stopping power (ENSP) for each case, helpful insights could be drawn.

In this computational campaign, SRIM-2013—in Quick Calculation mode—was used to calculate the displacements per atom (dpa) and ENSP for seven selected incident ions with varying energies: 1 MeV H, 1 MeV He, 3 MeV C, 2.4 MeV Mg, 2 MeV Al, 3.6 MeV Fe, and 4 MeV Zr. Each simulation used 10,000 ions to ensure statistical accuracy. The quartz (SiO_2) target density was set to 2.65 g/cm^3. Based on prior simulation studies [43], the displacement energies were set to 29 eV for Si and 71 eV for O, yielding an average displacement energy of 41.6 eV. Additional input parameters, including lattice binding energy and surface energy, were adopted based on the recommendations by Agarwal et al. [1] and are summarized in Table 3.

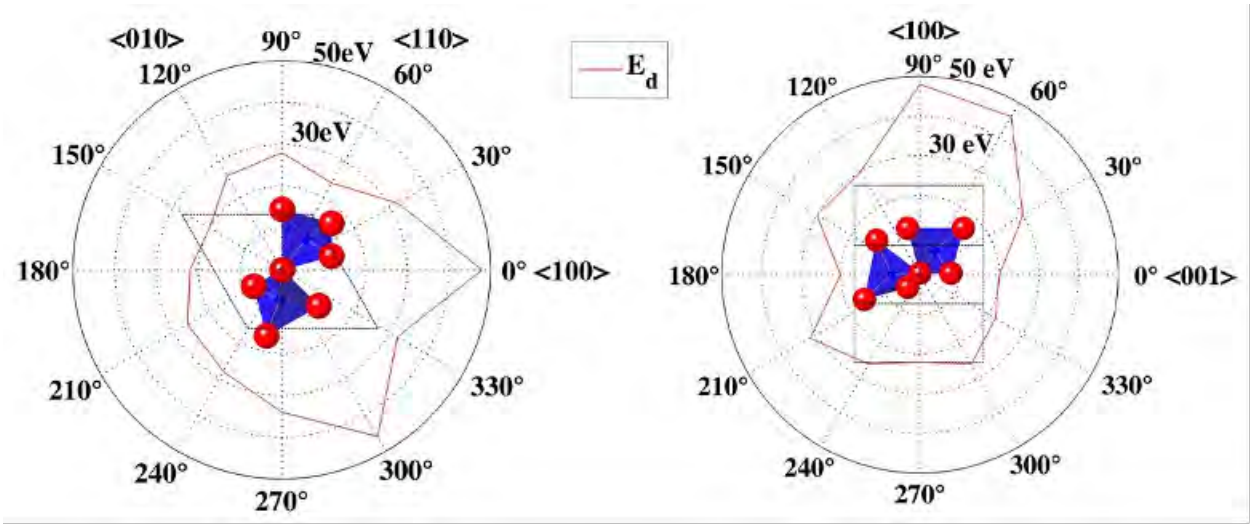

Figure 3. Threshold displacement energy of silicon in quartz along various crystallographic directions, calculated using molecular dynamics simulations [43].

SRIM employs Monte Carlo simulations based on the binary collision approximation, tracking the trajectory and velocity of both incident and recoil ions during collisions, while assuming straight-line paths between successive collisions [48]. It provides valuable predictions for ion implantation profiles, energy loss depth distributions (separated into electronic and nuclear components), dpa depth profiles, sputtering yields, and the total energy dissipated through ionization and phonon generation.

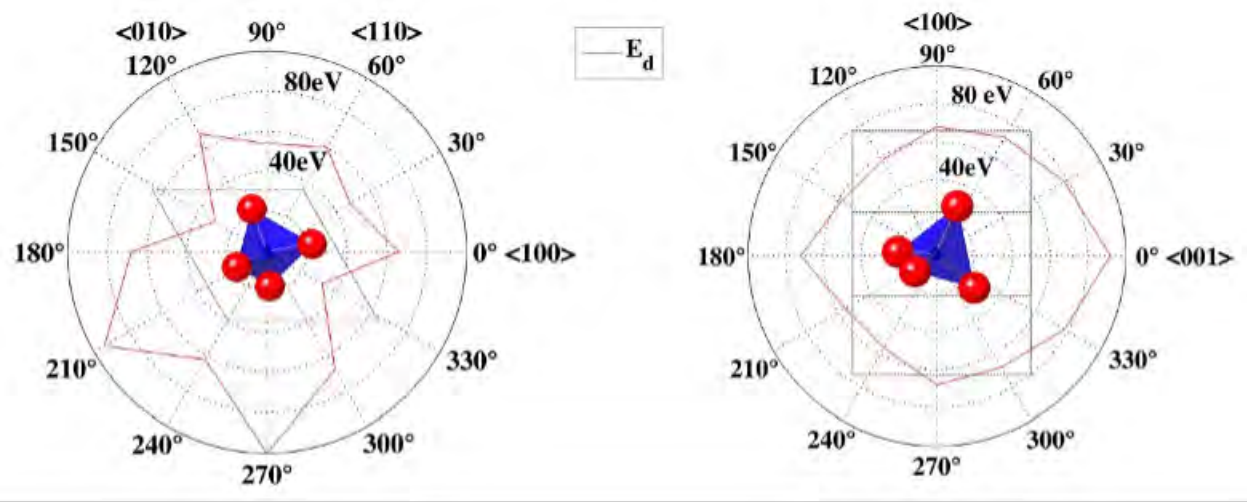

Figure 4. Threshold displacement energy of oxygen in quartz along various crystallographic directions, calculated using molecular dynamics simulations [43].

Table 3. Parameter settings for SRIM calculations of quartz (SiO_2) target

	Si	O
Displacement Energy	29 eV	71 eV
Lattice Binding Energy	2 eV	3 eV
Surface Energy	4.7 eV	2 eV

8.1 DISPLACEMENT CALCULATIONS

For irradiation studies, SRIM can estimate the average damage energy or the number of atomic displacements (vacancies) as a function of penetration depth. Based on the Norgett–Robinson–Torrens (NRT) model [30], the total number of displacements (i.e., vacancies) produced at a given depth can be calculated using:

$$\nu_{\mathrm{NRT}} = \frac{\kappa T_d}{2E_d}, \tag{1}$$

where κ is the displacement efficiency (typically 0.8), T_d is the damage energy, and E_d is the displacement threshold energy. Once the number of displacements is known, the dpa can be calculated as:

$$\mathrm{dpa} = \frac{\phi \times \nu}{\Omega}, \tag{2}$$

where ϕ is the ion fluence and Ω is the atomic density of the target material.

Assuming the same fluence of 10^{21} m^{-2}, the dpa values at a depth of 0.5 μm in the SiO_2 target were calculated for seven selected incident ions and are summarized in Table 4. Overall, heavier ions (higher Z) in the 1–4 MeV energy range produce higher dpa values under identical fluence conditions.

The dpa values can be further converted to MGy using the relation:

$$\mathrm{Gy} = \frac{\mathrm{dpa} \times \Omega \times E_d}{\rho}, \tag{3}$$

Table 4. Summary of ion irradiation conditions with a total fluence of 10^{21} $\mathbf{m}^{-2}$

Incident Particle	dpa	MGy	ENSP
1 MeV H	0.002	0.13	3598
1 MeV He	0.02	1.34	1614
3 MeV C	0.42	28.1	737
2.4 MeV Mg	2.78	185.9	63
2 MeV Al	4.27	285.6	37
3.6 MeV Fe	14.15	946.6	14
4 MeV Zr	36.25	2425.1	4
Fast fission spectra	–	–	3
Fusion first-wall spectra	–	–	6
Fast reactor external shielding	–	–	600–6000

where ρ is the mass density. For quartz, 1 dpa corresponds to approximately 66.9 MGy.

8.2 ELECTRONIC-TO-NUCLEAR STOPPING POWER ANALYSIS

For the electronic-to-nuclear stopping power (ENSP) analysis, ionization energy loss (i.e., electronic stopping) occurs as ions traverse matter and interact with target electrons, causing excitation or ionization. The electronic stopping power as a function of depth for the selected ions in Table 4 was obtained from the ionization energy loss in the SRIM output (Figure 5). Nuclear stopping power refers to the energy loss per unit path length due to elastic collisions between the incident ions and target nuclei (i.e., the total energy transferred to atomic nuclei).

To calculate the ENSP of quartz under neutron irradiation in nuclear reactors, it is important to note that neutrons are uncharged and do not undergo electronic or nuclear stopping in the same manner as charged particles. Instead, neutron irradiation causes damage through nuclear collisions that generate primary knock-on atoms (PKAs) [9], which then lose energy via electronic and nuclear stopping mechanisms within the material. Therefore, ENSP calculations apply to the PKAs but not the neutrons themselves. To obtain the average ENSP under neutron irradiation, the following integral over the neutron energy spectrum is used:

$$\mathrm{ENSP} = \frac{\int \phi(E_n) \cdot \mathrm{PKA}(E) \cdot \dfrac{S_e(E)}{S_n(E)}\, dE}{\int \phi(E_n) \cdot \mathrm{PKA}(E)\, dE} \tag{4}$$

where $\phi(E_n)$ is the neutron flux as a function of neutron energy E_n. PKA(E) is the number of PKAs produced per unit neutron fluence per unit energy. $S_e(E)$ and $S_n(E)$ are the electronic and nuclear stopping powers of the PKAs as functions of their energy E, respectively.

In the HFIR mixed-spectrum (thermal + epithermal) test reactor, PKAs typically range from 1–10 keV, with an average energy of ~3 keV, resulting in a mean ENSP for SiO_2 of ~0.6 (range: 0.4–1). In fast sodium-cooled fission reactors (e.g., FFTF, with an average neutron energy of ~0.7 MeV), PKAs span

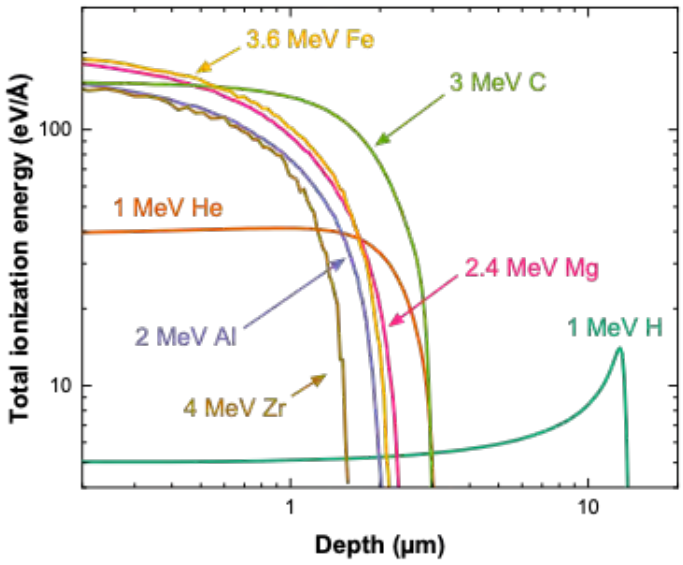

Figure 5. SRIM-calculated total ionization energy (electron stopping) versus depth for various ions implanted in quartz.

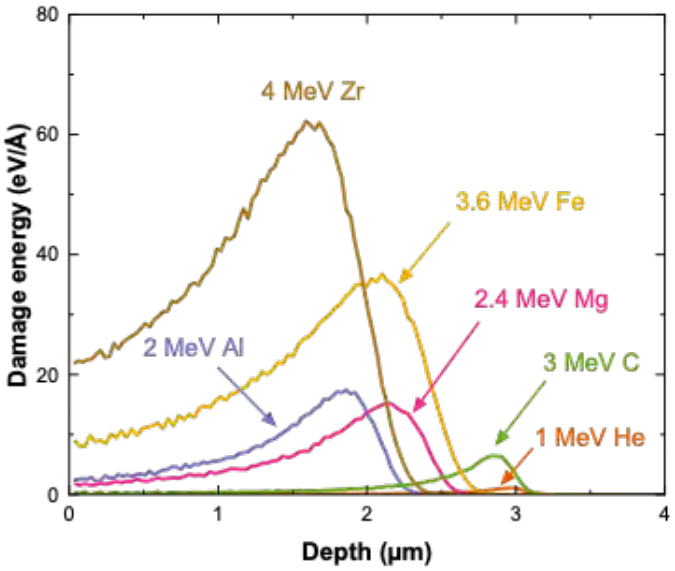

Figure 6. SRIM-calculated damage energy (nuclear stopping) versus depth for various ions implanted in quartz.

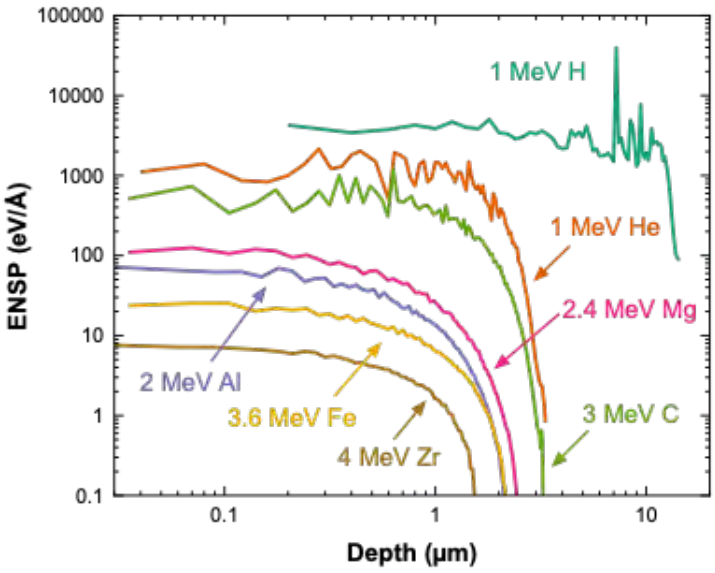

Figure 7. SRIM-calculated electronic-to-nuclear stopping power (ENSP) versus depth for various ions implanted in quartz.

20–120 keV (average ~50 keV), yielding ENSP ≈ 3 (range: 2–4). For fusion DEMO first wall conditions (14 MeV D–T peak), PKAs range from 80 keV to over 1 MeV (average ~200 keV), producing ENSP ≈ 6 (range: 5–8). In fast reactor external shielding, PKAs span a wide energy range depending on the distance from the core [17], with estimated ENSP values ranging from 600 to 6000. These values are summarized in Table 4. However, precise ENSP calculations for SiO_2 in specific reactor environments require detailed neutronics simulations that account for the full neutron energy spectrum.

Table 5. Irradiation parameters from selected literature on quartz RIVE.

Ion	Energy (MeV)	Dose (dpa)	Average ENSP	RIVE (%)	Ref
Na	0.05	~0.1	0.24	10.3	[13]
Si	3	~0.1	17	8.6	[23]
He	5.5	~0.1	1730	4.5	[35]
Na	0.05	~1	0.24	11.3	[13]
Si	3	~1	17	16.7	[23]
Ni	13	~1	17	14.3	[35]

To further investigate the effect of ENSP on RIVE, additional SRIM calculations were performed based on limited prior ion irradiation studies [13, 23, 35] that reported RIVE at comparable doses of ~0.1 and ~1 dpa. At ~0.1 dpa, a general trend of lower RIVE with higher ENSP is observed. However, this correlation is less clear at ~1 dpa, where RIVE ranges from 11% to 16% despite ENSP values between 0.24 and 17. A systematic study using different ion species and energies to vary ENSP would be valuable

for simulating the combined effects of neutron and gamma irradiation in quartz across different reactor types and locations, and for further clarifying the potential influence of gamma irradiation on RIVE.

8.3 SUMMARY OF INSIGHTS FROM ION IRRADIATION AND CORRESPONDING ENSP CALCULATIONS

The preliminary computational study presented herein provides helpful insights into possible interplay between neutron and gamma irradiation doses and their effects on observed RIVE. The following is a list of key observations.

- **Volume Expansion:** The degree of RIVE in quartz decreases with higher ENSP at lower doses (~0.1 dpa, which is roughly equivalent to 60–80 years of reactor exposure), but this correlation becomes less pronounced at higher doses (~1 dpa).
- **Dose-Dependent RIVE:** At ~1 dpa, RIVE varies across irradiation conditions, with volumetric expansion ranging from 11–16% for ENSP values between 0.24 and 17.
- **Heavier Ions and dpa:** Heavier ions (e.g., Zr, Fe) produce higher dpa values and significant localized damage under identical fluence, with Zr exhibiting the maximum dpa of 36.25 at 0.5 μm depth. Conversely, lighter ions (e.g., H, He) impart less dpa and are stopped predominantly by electronic stopping mechanisms.
- **Systematic Ion Studies:** The results suggest the need for systematic experimental studies using various ion species and energies to disentangle neutron- and gamma-induced effects.

9. CONCLUSIONS AND PERSPECTIVES

The observed neutron–flux dependence of radiation-induced volumetric expansion (RIVE) in concrete aggregate minerals has been investigated by considering mechanisms that could explain the effect, including the roles of accompanying γ irradiation and irradiation creep. A preliminary computational study (using SRIM to explore electronic–to–nuclear stopping power regimes) was also performed to illuminate the interplay between neutron and γ radiation doses.

The following conclusions can be drawn.

- **An evident neutron flux effect on RIVE exists at fixed fluence.** Higher neutron flux rates produce greater RIVE than lower flux at the same total fluence.
- **Time–assisted healing hypothesis.** At equal fluence, lower flux provides more time for concurrent healing (irrespective of the detailed flux dependence of each pathway). Both γ irradiation and irradiation creep can contribute time/flux–dependent recovery reducing overall observed RIVE.
- **Mineralogy matters.** RIVE is mineral/rock dependent: quartz exhibits the largest swelling (15–18%) upon crystalline–to–amorphous transformation with a strong flux effect; feldspar and granite also swell significantly (with differential phase swelling in granite inducing internal stresses); basalt/mafic aggregates swell less overall; mica swells anisotropically with early degradation; amphibole shows intermediate behavior. In all cases, it is expected that low flux mitigates damage via recovery, whereas high flux may not allow enough recovery time.

- **Multiple healing pathways can operate below 100°C.** (i) Point–defect recombination/migration (including H/OH–assisted reactions) proceeds slowly at ambient to modest temperatures; (ii) structural relaxation/viscous bond–rearrangement of amorphous SiO_2 has a very low activation barrier (∼0.13 eV), allowing gradual stress relaxation/compaction between cascade events; (iii) cascade thermal spikes can effect instantaneous local annealing.
- **Flux may shift the amorphization threshold.** Because recovery proceeds during irradiation at low flux, the critical dose for quartz amorphization may become higher at low flux and lower at high flux. Thus, time could inversely compensate for temperature in thermal annealing such that the amorphization threshold increases with irradiation temperature. Here, lower flux corresponds to high temperature (enabling more annealing) while higher flux corresponds to low temperature (limited annealing).
- γ **irradiation affects both damage and healing.** γ fields create E′ and NBOHC defects and, depending on $H/H_2/H_2O$ availability, enable chemically assisted passivation below 100°C (Si–H/Si–OH formation). With increasing temperature ($\gtrsim$150–300°C), intrinsic/thermally assisted annealing pathways dominate, further reducing steady–state defect populations.
- **Irradiation creep is operative well below 100°C.** In amorphous silica, radiation can generate defects and bond–switching events, aided by occasional cascade thermal spikes. This enables a Newtonian–like, athermal creep under load. All energetic radiation types can induce such creep (efficiency: neutrons/ions > electrons/γ), implying stress–assisted relaxation may contribute to the observed flux effect.
- **Preliminary SRIM–guided insights.** At low dose (∼0.1 dpa), RIVE in quartz clearly decreases with increasing ENSP, whereas at ∼1 dpa RIVE dependence on ENSP is less pronounced. Heavier ions (e.g., Zr, Fe) generate higher dpa and more localized damage at identical fluence; lighter ions (H, He) are dominated by electronic stopping. These trends motivate systematic ion–irradiation campaigns to disentangle neutron– and γ–driven contributions.

10. RECOMMENDATIONS FOR FUTURE WORK

- **Reactor-Specific Neutronics Modeling:** To refine ENSP predictions, detailed simulations that incorporate neutron flux spectra are necessary under various reactor conditions.
- **Ion-Irradiation Experimental Validation:** Systematic experiments with ion irradiation at varying doses, fluxes, and ENSP values will help clarify links among defect production mechanisms, flux effects, and resultant RIVE.

References

[1] S. Agarwal, Y. Lin, C. Li, R.E. Stoller, and S.J. Zinkle. On the use of srim for calculating vacancy production: Quick calculation and full-cascade options. *Nuclear Instruments and Methods in Physics Research Section B: Beam Interactions with Materials and Atoms*, 503:11–29, 2021.

[2] S. Agnello, R. Boscaino, G. Buscarino, and F.M. Gelardi. Modifications of optical absorption band of e_γ' center in silica. *Journal of Non-Crystalline Solids*, 351(21):1801–1804, 2005. SiO2, Advanced Dielectrics and Related Devices 5.

[3] Sebastian Bruns and Karsten Durst. Local crack suppression and activation of plastic flow via electron irradiation in oxide glasses. *Materials & Design*, 251:113726, 2025.

[4] V.N. Bykov, A.V. Denisov, V.B. Dubrovskii, V.V. Korenevskii, G.K. Krivokoneva, and L.P. Muzalevskii. Effect of irradiation temperature on the radiation expansion of quartz. *Atomnaya Energiya*, 51(3):593–595, September 1981.

[5] R.A.B. Devine. Macroscopic and microscopic effects of radiation in amorphous sio2. *Nuclear Instruments and Methods in Physics Research Section B: Beam Interactions with Materials and Atoms*, 91(1):378–390, 1994.

[6] Roderick A. B. Devine, J.-P Duraud, and E. Dooryhée. *Structure and imperfections in amorphous and crystalline silicon dioxide*. John Wiley, 2000.

[7] Qingyi Feng, Hongxiang Deng, Biyi Wang, Bo li, Xia Xiang, Li Li, Xiaodong Yuan, Wanguo Zheng, Hongdong Yang, Sean Li, and Xiaotao Zu. Neutron irradiation effect on amorphous porous silica. *Journal of the American Ceramic Society*, 105(12):7334–7343, 2022.

[8] Xing Gao, Yongnian Qi, Qing Mu, Ying Yan, and Ping Zhou. Propagation mechanism of e′-center and nbohc in fused silica induced by gamma-ray irradiation. *Opt. Mater. Express*, 14(10):2472–2487, Oct 2024.

[9] M.R. Gilbert and J.C. Sublet. Pka distributions: Contributions from transmutation products and from radioactive decay. *Nuclear Materials and Energy*, 9:576–580, 2016.

[10] Sylvain Girard, Antonino Alessi, Nicolas Richard, Layla Martin-Samos, Vincenzo De Michele, Luigi Giacomazzi, Simonpietro Agnello, Diego Di Francesca, Adriana Morana, Blaž Winkler, Imène Reghioua, Philippe Paillet, Marco Cannas, Thierry Robin, Aziz Boukenter, and Youcef Ouerdane. Overview of radiation induced point defects in silica-based optical fibers. *Reviews in Physics*, 4:100032, 2019.

[11] Malcolm Griffiths. Microstructural effects on irradiation creep of reactor core materials. *Materials (Basel)*, 16(6):2287, 2023.

[12] David L. Griscom. Optical properties and structure of defects in silica glass. *The Centennial Memorial Issue of The Ceramic Society of Japan*, 99(10), 1991.

[13] F. Harbsmeier and W. Boise. Ion beam induced amorphization in alpha quartz. *Journal of Applied Physics*, 83(8):4049–4054, 1998.

[14] S. Hirsch, H. Klein, and P. Jung. Dimensional changes of silica-, borosilicate- and germania-glasses and quartz under irradiation. *Journal of Non-Crystalline Solids*, 351(40):3279–3288, 2005.

[15] T. Thuy Hoang and Junhyeok Bang. Excitation induced mechanical softening and plastic deformation in sio_2 and al_2o_3. *J. Phys. Chem. C*, 129(15):7479–7484, 2025.

[16] Juan Huguet-Garcia, Aurélien Jankowiak, Sandrine Miro, Thierry Vandenberghe, Clara Grygiel, Isabelle Monnet, and Jean-Marc Costantini. In situ characterization of ion-irradiation enhanced creep of third generation tyranno sa3 sic fibers. *Journal of Materials Research*, 30(9):1572–1582, 2015.

[17] IAEA. Nuclear data services. Available online at https://www-nds.iaea.org/ [Accessed: Date Unknown].

[18] M. Jivanescu, A. Stesmans, and V. V. Afanas'ev. Multifrequency esr analysis of the$E_{\delta}^{'}$ defect in a-sio_2. *Phys. Rev. B*, 83:094118, Mar 2011.

[19] J.H. Konnert, P. D'Antonio, and J. Karle. Comparison of radial distribution function for silica glass with those for various bonding topologies: Use of correlation function. *Journal of Non-Crystalline Solids*, 53(1):135–141, 1982.

[20] Y. Le Pape, Alnaggar. M., E. Tajuelo Rodriguez, and A. Brooks. Irradiation effects on reinforced concrete structures – experimental and analytical study on irradiated concrete – steel bonding, modeling and simulation of structural response. Technical Report NUREG/CR-7312, Oak Ridge National Laboratory, 2025.

[21] Y. Le Pape, J. Sanahuja, and M.H.F. Alsaid. Irradiation-induced damage in concrete-forming aggregates – revisiting literature data through micromechanics. *Materials and Structures*, 53:35, 2020.

[22] Giuseppe Mattia Lo Piccolo, Marco Cannas, and Simonpietro Agnello. Intrinsic point defects in silica for fiber optics applications. *Materials*, 14(24), 2021.

[23] V.N. Luu, K. Murakami, H. Samouh, I. Maruyama, K. Suzuki, P. Prak Tom, L. Chen, S. Kano, H. Yang, H. Abe, and M. Suzuki. Swelling of α-quartz induced by mev ions irradiation: Critical dose and swelling mechanism. *Journal of Nuclear Materials*, 539:152266, 2020.

[24] I. Maruyama, O. Kontani, M. Takizawa, S. Sawada, S. Ishikawa, J. Yasukouchi, O. Sato, J. Etoh, and T. Igari. Development of the soundness assessment procedure for concrete members affected by neutron and gamma-irradiation. *Journal of Advanced Concrete Technology*, 15:440–523, 2017.

[25] Ippei Maruyama, Kenta Murakami, Takahiro Ohkubo, Shohei Sawada, Osamu Kontani, Takafumi Igari, Masaki Kawai, and Junji Etoh. Neutron flux impact on rate of expansion of quartz. *Journal of Nuclear Materials*, 606:155631, 2025.

[26] S. G. Mayr, Y. Ashkenazy, K. Albe, and R. S. Averback. Mechanisms of radiation-induced viscous flow: role of point defects. *Physical Review Letters*, 90(5):055505, 2003.

[27] F Messina, S Agnello, M Cannas, and A Parlato. Room temperature instability of e'γ centers induced by gamma irradiation in amorphous sio_2. *J. Phys. Chem. A*, 113(6):1026–1032, 2009.

[28] F. Messina and M. Cannas. Stability of e' centers induced by 4.7ev laser radiation in sio2. *Journal of Non-Crystalline Solids*, 353(5):522–525, 2007. SiO2, Advanced Dielectrics and Related Devices 6.

[29] Kenta Murakami, Nhut luu vu, Takahiro Ohkubo, Sho Kano, Masami Nishikawa, Kiyoteru Suzuki, and Ippei Maruyama. Relationship between ion irradiation-induced amorphization and volume expansion in quartz and feldspars for concrete aggregates. *Journal of Nuclear Materials*, 602:155326, 12 2024.

[30] M.J. Norgett, M.T. Robinson, and I.M. Torrens. A proposed method of calculating displacement dose rates. *Nuclear Engineering and Design*, 33(1):50–54, 1975.

[31] Laura Nuccio, Simonpietro Agnello, and Roberto Boscaino. Role of h_2O in the thermal annealing of the e'_γ center in amorphous silicon dioxide. *Phys. Rev. B*, 79:125205, Mar 2009.

[32] N Ollier, I Reghioua, O Cavani, M Mobasher, A Alessi, S le Floch, and L Skuja. Probing densified silica glass structure by molecular oxygen and e' center formation under electron irradiation. *Scientific Reports*, 13(1):13657, 2023.

[33] I. Pignatelli, A. Kumar, K.G. Field, B. Wang, Y. Yu, Y. Le Pape, M. Bauchy, and G. Sant. Direct experimental evidence for differing reactivity alterations of minerals following irradiation: The case of calcite and quartz. *Scientific Reports – Nature*, 6(20155):1–10, January 2016.

[34] W Primak. Fast-neutron-induced changes in quartz and vitreous silica. *Physical Review*, 110(6):1240–1254, 1958.

[35] Z. Qi, X. Chen, A. Bouissonnié, E.T. Rodriguez, Y.L. Pape, M.L. Crespillo, G. Sant, and S.J. Zinkle. Investigation of ion irradiation effects on mineral analogues of concrete aggregates. *Journal of Nuclear Materials*, 605:155539, 2025.

[36] Morgan Rusinowicz, Sergio Sao-Joao, Matthieu Bourguignon, Gustavo Rosales-Sosa, Yoshinari Kato, Fabien Volpi, Etienne Barthel, and Guillaume Kermouche. Electric charges as an apparent governing parameter for electron induced stress relaxation in amorphous silica micropillars. *Scripta Materialia*, 261:116628, 2025.

[37] S. Sabatino, A. Brooks, P. Bran Anleu, D. Arregui Mena, M. Rivers, E. Tajuelo Rodriguez, and Y. Le Pape. Assessment of neutron-induced crack volume on aggregates of varied mineralogy and estimation of irradiation damage depth in the concrete biological shield. Technical Report ORNL/SPR-2024/3581, Oak Ridge National Laboratory, June 2024.

[38] N.J. Simon. Irradiation damage in inorganic insulation materials for iter magnets: A review. Technical Report NISTAR 5025, National Institute of Standards and Technology, 1994.

[39] H. Trinkaus. Local stress relaxation in thermal spikes as a possible cause for creep and macroscopic stress relaxation of amorphous solids under irradiation. *Journal of Nuclear Materials*, 223(2):196–201, 1995.

[40] H. Trinkaus. Anisotropic creep and growth of amorphous solids under swift heavy ion bombardment: An asymptotic thermal spike approach. *Nuclear Instruments and Methods in Physics Research Section B: Beam Interactions with Materials and Atoms*, 107(1):155–159, 1996.

[41] H. Trinkaus. Thermal spike model for irradiation creep of amorphous solids: Comparison to experimental data for ion irradiated vitreous silica. *Journal of Nuclear Materials*, 246(2):244–246, 1997.

[42] Nhut Luu Vu. *On the Behavior of Siliceous Minerals under Irradiation and Plant Life Management of Concrete Structure in Nuclear Facilities*. PhD thesis, Nagaoka University of Technology, 2021.

[43] B. Wang, Y. Yu, I. Pignatelli, G. N. Sant, and M. Bauchy. Nature of Radiation-Induced Defects in Quartz. *The Journal of Chemical Physics*, 143:024505, April 2015.

[44] William E. Windes, David T. Rohrbaugh, and W. David Swank. Agc-3 irradiation creep strain data analysis. Technical report, Idaho National Laboratory, Jul 2019. Prepared for U.S. Department of Energy, Office of Nuclear Energy.

[45] Jonathan J. Witcher, Wilbur J. Reichman, Luke B. Fletcher, Neil W. Troy, and Denise M. Krol. Thermal annealing of femtosecond laser written structures in silica glass. *Opt. Mater. Express*, 3(4):502–510, Apr 2013.

[46] Y. Zhang, S. Dillon, and J. Lambros. Creep characterization of amorphous sio_2 in the transmission electron microscope using digital image correlation and finite element analysis. *Experimental Mechanics*, 63(4):621–636, 2023.

[47] Kun Zheng, Chengcai Wang, Yong-Qiang Cheng, Yonghai Yue, Xiaodong Han, Ze Zhang, Zhiwei Shan, Scott X Mao, Miaomiao Ye, Yadong Yin, and Evan Ma. Electron-beam-assisted superplastic shaping of nanoscale amorphous silica. *Nature Communications*, 1(1):24, 2010.

[48] J.F. Ziegler and J.P. Biersack. *The Stopping and Range of Ions in Matter*. Treatise on Heavy-Ion Science: Volume 6: Astrophysics, Chemistry, and Condensed Matter. Springer US, Boston, MA, 1985.

[49] Sezer Özerinç, Robert S. Averback, and William P. King. In situ creep measurements on micropillar samples during heavy ion irradiation. *Journal of Nuclear Materials*, 451(1):104–110, 2014.